RESEARCH REPOSITORY

Barmi, M.J. and Minakshi, M. (2016) Tuning the redox properties of the
nanostructured CoMoO4 electrode: Effects of surfactant content and
synthesis temperature. ChemPlusChem, 81 (9). pp. 964-977.

http://researchrepository.murdoch.edu.au/id/eprint/32376/

Accepted Article

Title: Tuning the redox properties of nanostructured CoMoO4 electrode: Effects of surfactant contents and synthesis temperature

Authors: Maryam Barmi; Manickam Minakshi

A Journal of

ChemPubSoc
Europe

Tuning the redox properties of nanostructured CoMoO$_4$ electrode: Effects of surfactant content and synthesis temperature

Maryam Jozegholami Barmi and Manickam Minakshi*

School of Engineering and Information Technology, Murdoch University, WA 6150, Australia

Abstract

A systematic study was performed to examine the effects of surfactant content and synthesis temperature on the morphologies and the redox properties of cobalt molybdate (CoMoO$_4$). Results revealed that while varying the concentration of surfactant (F127) the morphology varies from nanorods, to nanospheres and nanoneedles. The concentration of metal to surfactant ratio with 1:1 outperform in specific capacitance, energy density and cycling stability than that of 1:0.5 and 1:2 ratios. The surfactant at the optimised ratio significantly influenced the morphology and particle size of the CoMoO$_4$ material and act as a template whereas increasing the synthetic temperature did not contribute much to the energy storage. Asymmetric supercapacitor is fabricated based on CoMoO$_4$ as positive electrode and activated carbon as negative electrode in 2 M NaOH electrolyte. The CoMoO$_4$ material synthesised at 300 ^{o}C in the presence of F127 (1:1) showed specific capacitance of 79 F g^{-1} and energy density of 21 W h $\cdot$ kg^{-1} when tested as a hybrid device. This suggests the redox activity and its storage capability depend on the surfactant content as well as it's self-assembly behaviour. CoMoO$_4$ showed excellent cycling stability retaining over 75 % of its initial capacitance after 2000 cycles which makes it a very promising candidate for large scale energy storage applications.

*E: *minakshi@murdoch.edu.au*

1. Introduction

Supercapacitors also known as electrochemical capacitors are the energy storage devices found widespread applications including electronic gadgets, power backup systems, hybrid electric vehicles and medical appliances.[1-4] They have been considered as alternative power sources since they possess higher power density and longer life cycle than conventional batteries, and also they have higher energy density than dielectric capacitors.[5] Over a decade, demand for renewable energy has been increased and energy storage devices have been extensively explored as the renewable energy production is intermittent. Storing energy is necessary because capturing a small percentage of potential wind and solar energy could contribute significantly to meet the world's electrical energy requirement. Much effort has been devoted to develop new electrode materials and enhance its performance in order to satisfy the new energy demand.[6-15] At present, to meet these requirements, transition metal oxides and phosphates have been identified to exhibit superior redox activity and thus a high storage capability can be obtained at a relatively low cost.[6, 7] Transition metal oxides[6] and phosphates[7] are well known in the field for over two decades now, whereas molybdates [8-15] are evolving recently. Metal molybdates, [8, 11] $AMoO_4$ – type compounds (where A is the divalent metal ion), are an interesting material due to their potential application in many fields including energy storage. Hence, much effort has been taken to synthesize nanostructured molybdate as electrodes for high performance supercapacitors.[8] A variety of molybdate materials such as $MnMoO_4$,[9] $CoMoO_4$,[11] $NiMoO_4$,[16] and $FeMoO_4$[17] have been developed and tested for energy applications.

Recently, metal molybdates such as $CoMoO_4$ [11] and $NiMoO_4$ [16] have demonstrated enhanced electrochemical performance over the oxide and phosphate counterparts. Cobalt molybdate ($CoMoO_4$) nanoparticles [18] synthesised via co-precipitation method were reported to have an effect on the particle size for samples annealed at elevated temperatures. In another

study, $CoMoO_4 \cdot 9H_2O$ nanorods[19] synthesised via hydrothermal method showed specific capacitance of 326 F g^{-1} at 5 mA cm^{-2}. The high capacitance was attributed to the rapid transportation of ions into the bulk of one dimensional material structure. To further improve the electrochemical performance of cobalt molybdate material, $CoMoO_4$/graphene composite[13] was synthesised via hydrothermal route. The composite showed enhanced specific capacitance and energy density of 168 F g^{-1} and 8 W h $\cdot$ kg^{-1}, respectively. In a different study, based on polymer coating, $CoMoO_4 \cdot 0.75H_2O$ has been coated with polyaniline (PANI)[10] to enhance the electrochemical properties of the material for energy storage applications. The $CoMoO_4$ coated with PANI nanorods showed specific capacitance of 380 F g^{-1} at a current density of 1 A g^{-1}. Further to the single electrode studies, the performance characteristics reported for the hybrid device (two electrodes system) constructed from AC vs. $CoMoO_4$ [20] showed specific capacitance of 105 F g^{-1} with an energy density of 14.5 W h $\cdot$ kg^{-1} when performed at a current density of 5 mA cm^{-2}. Interestingly, $CoMoO_4$ modified with chitosan [11] exhibiting a specific capacitance of 81 F g^{-1} were reported when used as a device at 3 A g^{-1} but with improved energy density of 25 W h $\cdot$ kg^{-1}. The enhanced energy density was attributed to the ability of chitosan adhesion to the molybdate moiety of $CoMoO_4$. However, the polymer modified $CoMoO_4$ may not be suitable for large scale applications. To conclude, all the aforementioned studies confirm that $CoMoO_4$ as a promising candidate for high performance supercapacitors because of the metal molybdate is low cost, environmentally friendly and abundant in resource. Nevertheless, to the best of our knowledge, the use of novel Pluronic F127 surfactant with an effect to the synthesis temperature and its physicochemical properties are not reported. However, a preliminary study on F127 surfactant in the $CoMoO_4$ has been reported in one of our earlier publications.[14] The significance and novelty of the current work lies in understanding the effects of the metal to surfactant ratio and the synthesis temperature both influencing the

change in morphology and enabling to tune the redox properties which collectively enhances the specific capacitance of $CoMoO_4$ than those reported for this material the literature. [11, 14] The contribution to the increment of the capacitance and its mechanism is proposed in this work.

With this in mind, current study has been pursued to understand the physico- and electrochemical properties of transition metal cation (Co) in the molybdate. In particular, insights into the redox behaviour and chemical stability of the Co are essential to enhance the energy storage. The morphology of the $CoMoO_4$ is also shown to be one of the most important factors in improving the electrochemical performance of the supercapacitors. We report here, tuning the redox properties of $CoMoO_4$ with varying the particle shape through altering the amount of surfactants. This is primarily related to the surface adsorption of surface active molecules on nucleating centres and thus tailoring the overall shape. The surfactant chosen for this study is Pluronic F127 commonly known as F127 has been regarded as a structure directing agent for synthesising oxide based materials. [21] We have adopted this unique surfactant for molybdates during the *in-situ* chemical synthesis. The optimised concentration of the surfactant ratio in this study (metal atom to F127 ratio; 1:1) acts as a soft template to allow uniform growth of hierarchical nanospheres without which it resulted in agglomerated nanorods due to uncontrolled Ostwald ripening effects.[22-23] The X-ray photoelectron spectroscopy analysis for the nanospheres with surfactant ratio (1:1) indicates a carbon surface group deposits (decomposed product of F127) on the surface whereas the remaining samples have not indicated this surface behavior.

Our current study suggests that nanospheres possessing higher surface area is desirable for high adsorption/desorption of ions while tuning the $Co^{2+/3+}$ redox couple. At the critical micelle concentration (CMC), the bulk concentration of the individual surfactant molecules reaches the saturation level and determines the morphology and the size of the

synthesized particles. Here in this study, we have also extended our work to examine the influence of synthesis temperature (between 300 °C and 500 °C), on the particle size, structure and morphology of $CoMoO_4$ material. To the best of our knowledge, this is the first study of employing F127 surfactant in cobalt molybdate relating to the change in morphology and electrochemistry for energy storage devices. We have shown that hierarchical $CoMoO_4$ nanospheres exhibit higher specific capacitance and better longevity constituting both faradaic and non-faradaic processes. The potential impact of energy storage through the aid of scalable nanostructured materials has been demonstrated in our work.

2. Results and Discussion

2.1 Effect of surfactant content on morphology and redox properties of synthesized $CoMoO_4$

(a) Physicochemical Characterization

X-ray diffraction patterns of the $CoMoO_4$ synthesized with different surfactant loadings (metal to surfactant ratio 1:0.5; 1:1; and 1:2) are shown in Fig. 1. All the diffraction patterns are in agreement with the diffraction peaks given in the JCPDS card no. 21-0868 indicating the formation of single phase $CoMoO_4$ material. The major diffraction peak at 26.5° observed for all XRD patterns can be assigned to (002) plane of $CoMoO_4$ along with several other minor reflections in different orientations labelled in the pattern indicates a polycrystalline in nature. The crystallite size of ~ 10.1 nm was calculated by the Debye-Scherer formula using the major diffraction peak (002) having full-width at half-maximum (FWHM) as 0.91°. It can be seen from the Fig. 1 that $CoMoO_4$ samples synthesised with a different surfactant loadings showed no distinct changes in their peak positions, implying the structure is intact. However, as the surfactant loading increased from 0.5 to 1 (in Fig. 1b), all the peaks become well defined, becoming sharper with increasing intensity, shows the material is more crystalline with a higher degree of ordering in nature. While increasing the loading to 2.0 (in Fig. 1c), no

further changes in the diffraction patterns are visible, indicating that the saturation content of F127 in $CoMoO_4$ could be around 1.0 loading.

To analyse the surface morphology of the $CoMoO_4$ synthesized with different surfactant loadings, field emission scanning electron microscopy (FE-SEM) has been employed and the images are shown in Fig. 2. For comparison, image for the surfactant – free $CoMoO_4$ is also shown. It can be seen from Fig. 2a, for the surfactant-free $CoMoO_4$, the surface morphology is aggregated possessing a rod-shaped structure of ~ 2 µm in length. The effect of surfactant addition with different loadings shows significant changes in the morphology (Fig. 2b-d). For 0.5 loading (Fig. 2b), the aggregated rod-shaped form changed to a more dispersed fashion of nanorods with < 1 µm in length. However, the surface morphology comprises a large portion of irregular length of nanorods in an aggregated form. After 1.0 loading, nanorods transformed to hierarchical nanospheres (Fig. 2c) with around 1− 1.5 µm in diameter. When the concentration of the surfactant is increased to 1.0 loading and reached the CMC value, the individual surfactant molecules tend to form micelles in well-defined clusters that reduces the number of nanorods by grouping them into a sphere like blocks (Fig. 2c).[24] The adsorption site at the edges of the nanorods becomes less reactive for further nucleation and led to a circular growth in the formation of spheres.[25] The BET analysis showed an increase in the surface area (from 20.2 to 30.6 $m^2.\ g^{-1}$) and porosity for this loading (Fig. S1, ESI§) demonstrates that the surfactant molecules were adsorbed in between the layers of $CoMoO_4$ structure. This is evident that the increase in concentration, rearranges the surfactant molecules to induce shape transformation from nanorods to nanospheres. For 2.0 loading, the FE-SEM image of the product (Fig. 2d) showed nanoneedles having a uniform length but loosely packed.

This confirms the fact that Co^{2+} and MoO_4^{2-} ions distributed in the solution containing the surfactant F127 behaves like a template and tends to self-assemble to form micellar

structure. After heating these precursors, the given temperature contributed to the formation of nanorods, nanospheres or nanoneedles. It is reported in the literature that nanospheres possess higher electrical conductivity than the nanorods.[26] To satisfy increasing demands for large energy density and high power capability in energy storage devices, a porous nanosphere material that can accommodate fast transport of ions has been widely used.[27] The porous nanostructure with a higher surface area obtained at 300 ^{o}C in the presence of the given concentration of the surfactant would be crucial to achieve a high capacitance (discussed in the next section 2.2).[5]

The morphology of the as-synthesized products was further characterized by transmission electron microscopy (TEM) technique. Figures 3 - 5 show the representative TEM images of the $CoMoO_4$ products synthesized with different surfactant loadings. As shown in Fig. 3a, for 0.5 loading, the nano-rod like morphology with a diameter of about 50 nm and 1 μm in length was observed from TEM which is in good agreement with the SEM images (Fig. 2). The magnified view of this image (Fig. 3b) indicates an internal stress has been created during the synthesis process.[28] The high-resolution TEM (HRTEM) and its corresponding selected area diffraction pattern (SADP) taken from the individual nanorod are shown in Fig. 3c-d. The blurred lattice fringes and the diffused rings of $CoMoO_4$ material clearly ascertain the low crystallinity. The results obtained from the TEM imaging are in accordance with the XRD patterns (Fig. 1a) that the synthesized $CoMoO_4$ is amorphous. The energy dispersive analysis (EDS), Table 1, suggests that the samples were composed of mainly Co, Mo, and O. Figure 4 shows the TEM images of the surfactant loading 1.0. Rounded particles are seen in the TEM image (Fig. 4a) and its magnified view showed, interestingly, hexagonal shaped crystallites (Fig. 4b) stacked in a stairway like structure. The HRTEM image (Fig. 4c) taken from the hexagonal shaped individual crystallite shows lattice fringes and its corresponding SADP pattern (Fig. 4d) illustrates a series of well-defined rings

both confirming the $CoMoO_4$ product having 1.0 surfactant loading is a crystalline material. For surfactant loading 2.0, the TEM images are shown in Fig. 5. Nanoneedle like particles with diameter of 25 nm and < 1 μm in length are depicted from Fig. 5a. The magnified view of the nanorods (Fig. 5b) shows the microstructure composed of a rich defects and some contrast in the image corresponds to dislocations.[29] The defects and microtwinning are caused from the higher amount of surfactants in the solution. The HRTEM and its corresponding SADP pattern (Figs. 5c-d) indicate its polycrystalline characteristics. The results agree well with that of XRD investigation and FE-SEM images, discussed earlier in the section (Figs. 1 and 2). The microscopy images clearly show that varying the concentration of surfactant is a direct way of controlling the particle's shape that can led to suitable morphologies which is in accordance with the published work on the surfactant.[25]
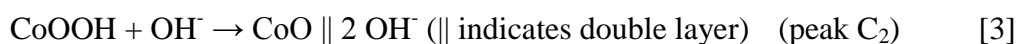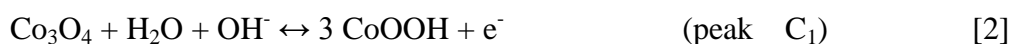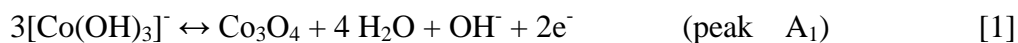
To study the elemental composition present in the synthesized $CoMoO_4$ and to evaluate the chemical state on the influence of surfactant loadings, X-ray photoelectron spectroscopy (XPS) has been used. The XPS spectra over regions specific to elements of our interest were recorded over five sweeps and the high-resolution spectra are plotted in Fig. 6. It presents the high-resolution C 1s, O 1s, Co 2p and Mo 3d of the $CoMoO_4$ sample with a lower surfactant ratio (1:0.5) loading. The C 1s spectrum in Fig. 6 can be deconvoluted into three individual component peaks located at 284.7, 286.9 and 289.0 eV assigned to C-C, C-O-C and O-C=O bonds, respectively.[30] The peaks at 284.7 and 286.9 eV can be assigned to hydrocarbons and the other one at 289 eV could be assigned to carbon associated from F127 surfactant. The O 1s spectrum in Fig. 6 located at 531 and 532 eV are assigned to metal oxides while the shoulder peak at 534 eV assigned to O-C=O bond. The asymmetrical and broad shape of the O 1s peaks verify the presence of OH^- groups adsorbed on the surface. The Co $2p_{1/2}$ and Co $2p_{3/2}$ split spin orbit components have been observed (Fig. 6) at 797 and 781 eV, respectively which is quite similar to those reported for this material.[31] A satellite peak

for these two components is also observed. The Mo 3d core-level spin-orbit doublets (at 232 eV and 235 eV) are also shown in Fig. 6 which is in accordance with the reported value of having a splitting width 3.0 eV. [32] Overall, the observed elemental compositions are in consistent with the database confirming the synthesized material is $CoMoO_4$. Interestingly, the elemental compositions for Co, Mo and O changes upon increasing the surfactant loadings and the results obtained from elemental dispersive analysis (EDS) are tabulated in Table 1 for ratios 1:0.5 and 1:1. It is worth noting from XPS that a 0.6 eV shift of the binding energy takes place with an increase in intensity for the peak corresponding to O-C=O at 288.4 eV in the optimised surfactant ratio (1:1) shown in (Fig. S2, ESI§). This provides us evidence that the carbon functional groups could increase the interaction between the $CoMoO_4$ particles and adsorption/desorption of ions thus contribute to higher specific capacitance. For the surfactant content loading 2.0, the ratio of the peak intensities between the hydrocarbon and carbon associated from the F127 start to decrease as illustrated in (Fig. S2, ESI §) indicating the optimised content of the surfactant could be 1.0.

(b) Electrochemical Characterization

The hybrid device, coupling cobalt molybdate with activated carbon, is considered a promising approach to enhance the electrochemical performance of capacitors. To evaluate this electrochemically, $CoMoO_4$ synthesized at 300 ^{o}C with a different surfactant loading was tested as a single electrode and then fabricated as a device to corroborate its suitability for energy storage devices. The cyclic voltammetric (three cell experiments) measurements of the $CoMoO_4$ nanorods, nanospheres and nanoneedles as electrodes were carried out at a scan rate of 1 mV s^{-1} in 2 M NaOH aqueous electrolyte and the results are displayed in Fig. 7. As can be seen in Fig. 7a-c, all the CV profiles invariably consist of two reduction peaks (C1 and C2) and one oxidation peak (A1) suggesting the $CoMoO_4$ electrode undergoes only one oxidation process and the product formed during the oxidation undergoes two separate

reductions during the reverse cathodic scan. The scan was initiated at 0 V going in the anodic direction to + 0.7 V and then reversing it back to the starting potential. The reaction mechanism involved can be discussed in the following way. When $CoMoO_4$ electrode is introduced in the alkaline electrolyte with a pH of over 9.0, as reported in the literature [9, 19] and Pourbaix (E_H - pH) diagram, it is oxidised in air to form cobaltous hydroxide ($Co(OH)_3$) prior any electrochemical measurements. During the anodic scan, $Co(OH)_3$ is oxidised to form Co_3O_4. In the reverse scan, Co_3O_4 undergoes a change in the reduction state of the Co atom in $CoMoO_4$ governed by faradaic reactions. The reactions corresponds to the redox peaks are as per the following equations (1-3)

$$3[Co(OH)_3]^- \leftrightarrow Co_3O_4 + 4\ H_2O + OH^- + 2e^- \qquad (\text{peak} \quad A_1) \qquad [1]$$

$$Co_3O_4 + H_2O + OH^- \leftrightarrow 3\ CoOOH + e^- \qquad (\text{peak} \quad C_1) \qquad [2]$$

$$CoOOH + OH^- \rightarrow CoO \parallel 2\ OH^- (\parallel \text{ indicates double layer}) \quad (\text{peak } C_2) \qquad [3]$$

The electrochemical behaviour of $CoMoO_4$ in Fig. 7 exhibits the quasi reversible faradaic process that involves electron transfer process in $Co^{2+/3+}$ redox couple [11] involving the ability of OH^- to be reversibly intercalated into the oxidised form of $CoMoO_4$ (Co_3O_4) for the improved charge storage (forming COOH) which is attributed to pseudocapacitance. However, the peak C_2 (Eq. 3) is raised from the formation of cobalt oxide (CoO) [33] and adsorption of ions on the near-surface corresponding to the non-faradaic process which is not reversible during the oxidation process but contributes to the capacitance. The above studies indicate that reduction of Co_3O_4 is reversible while the further reduction of CoOOH forms a mixture of CoO and adsorption of OH^- ions which is irreversible. Hence, the observed specific capacitance is from both the faradaic (Eqs. 1-2) and non-faradaic reaction (Eq. 3). For nanospheres (Fig. 7b), ratio of the reduction peaks C1 to C2 is higher than nanorods and nanoneedles suggesting the electrochemical properties are related to the size and morphologies. [34] When the material is subjected to continuous cycling in the potential region

0.0 to 0.7 V, the behaviour of the redox peaks are almost identical indicating the material could be reversibly oxidised/reduced over a number of cycles. On a close examination, comparison of nanostructured $CoMoO_4$ materials in Fig. 7d, reveals that the reduction/oxidation peaks are shifted to different potential regions. The C1 and C2 peaks occurred at less positive potentials with a difference of 0.2 V while anodic potential difference of 0.05 V have been observed for the samples synthesized at higher surfactant ratios (1.0 and 2.0). This suggests the redox activity and its potential depend on the arrangement of surfactant molecules as well as it's self-assembly behaviour. [23-25] The area under the peak is found to be higher for nanospheres indicating the fast electronic and ionic transport for the $CoMoO_4$ material [9] with the optimised surfactant ratio. This suggests highly crystalline in nature and smaller particle size material (nanorods and nanoneedles) are not favouring the electrochemical capacitance behaviour. The larger specific area for spheres contributes to the void space between the layers that aids the diffusion of OH^- ions into the electrode which resulted in high intense redox peaks (Fig. 7b).[27] Overall, from the cyclic voltammetric studies, nanospheres exhibited a capacitance of 170 F g^{-1} which is higher than that obtained for nanorods (85 F g^{-1}) and nanoneedles (125 F g^{-1}). Figure 8 (a – c) shows the galvanostatic charge-discharge curves of the $CoMoO_4$ electrodes at various current densities from 0.1 to 1 A g^{-1}. The higher surfactant loadings in Fig. 8 (b – c) exhibit a broad and symmetrical shape at a lower current density indicating excellent coulombic efficiency and reversibility of the material. The observed plateau-like region in charge-discharge curves around 0.5 V represents a pseudocapacitive in nature corresponding to $Co^{2+/3+}$ redox couple. The calculated specific capacitances of the optimised surfactant loading (1.0) were 204, 180, 154 and 100 F g^{-1} at discharge current densities of 0.1, 0.2, 0.5 and 1.0 A g^{-1}, respectively. The decrease in available specific capacitance at high current densities suggests the kinetics of a slow electron transfer and adsorption/desorption reactions during the redox process.

However, at a high current density of 1.0 A g^{-1}, 50% of the capacitance is still retained. The surfactant loadings of 0.5 and 2.0 delivered reversible capacitances of 105 and 175 F g^{-1} at discharge current density of 0.1 A g^{-1} which is 51% and 85% of the value obtained for the optimised content. At a higher current rate, the available capacitance was gradually dropped for the 0.5 and 1.0 loadings. Therefore, the optimum F127 content in the CoMoO$_4$ powder is 1.0.

To further qualify the synthesized CoMoO$_4$ in terms of the best surfactant content, galvanostatic (charge-discharge) and potentiostatic (CV) measurements were carried out in an asymmetric hybrid device with an electrochemical window of 1.6 V at a constant charge/discharge current of 0.2 A g^{-1} and varying scan rates ranging from 1 to 10 mV s^{-1}. This is beneficial to evaluate the practicality of CoMoO$_4$ in capacitor applications. A schematic representation of the hybrid device is shown in Fig. 9.

Figure 10A shows the galvanostatic discharge – charge profiles of the CoMoO$_4$ nanorods, nanospheres and nanoneedles and their cycling stability. The results for the first charge – discharge cycle for all the cells are shown in Fig. 10A. The symmetric behavior with low internal resistance (IR drop) confirms the excellent supercapacitive behavior for the samples synthesized at surfactant loadings 1.0 and 2.0. CoMoO$_4$ synthesized at a surfactant loading 1.0, showed a charge plateau like curve at 1.3 V and discharge plateau like curves at 1.3 V and 0.4 V regions indicating a reversible process and supporting the cyclic voltammetry data shown in Fig. 7b. The 1.3 V and 0.4 V regions could be attributed to the non-faradaic and faradaic (redox) mechanism corresponding to Co$^{3+/2+}$. The electrochemical capacitance is proportional to the time taken for the discharge.[8] From galvanostatic studies, using the equations (4 - 5), specific capacitance for nanorods, nanospheres, and nanoneedles were calculated [8] to be 36, 79 and 42 F g^{-1} having energy densities 8, 21 and 10 W h · kg^{-1}.

$$SC \ (F \ g^{-1}) = I \ \Delta t / m \ \Delta V \qquad\qquad Eq. \qquad (4)$$

$$E \ (W \ h \ kg^{-1}) = \frac{1}{2} \ SC \ \Delta V^2 \qquad\qquad Eq. \qquad (5)$$

where SC is the specific capacitance (F g^{-1}) , *I* is the current (A) imposed to the cell for

charge / discharge, Δt is the time taken to discharge in seconds (calculated from the discharge

curves), *m* is the weight of the active electrode (CoMoO$_4$) in g, and ΔV is the voltage window

(V). To maintain the charge balance of the hybrid cell, the mass of the active materials are

kept at 11.25 (CoMoO$_4$) and 21.6 (AC) mg. The total mass of the two electrodes in the hybrid

capacitor is 32.85 mg. Among the samples studied, the best performed nanosphere sample

with a surfactant loading of 1.0 was further tested for longevity measurements up to 2000

cycles at a discharge current density of 0.2 A g^{-1}. The specific capacitance versus cyclability

is shown in Fig. 10B. The hybrid device showed an excellent cycling stability with retention

of over 75% of its initial capacitance after 2000 cycles. The loss in capacitance is generally

explained by the versatility of the host CoMoO$_4$ material during the faradaic reactions

process. The inset in Fig. 10B shows the first and 2000th cycle of the sample. The

charge/discharge curves are symmetric and fully reversible after multiple cycles. The CV

curves of the hybrid capacitor device possessing nanorods, nanospheres and nanoneedles at

various scan rates (1, 2, 5 and 10 mV s^{-1}) were shown in Fig. 8 (d – f). The safe voltage

window was found to be 1.6 V. The redox behaviour for the hybrid device is quite similar to

those observed for single electrode (in Fig. 7) with one oxidation and two reduction peaks.

Upon increasing the scan rate from 1 to 10 mV s^{-1}, the current increased, the anodic peak

(A1) shifted towards positive potential and the cathodic peaks (C1 and C2) shifted towards

negative potential. The observed peak current and the area under the curve increased in a

linear fashion with the scan rate illustrating the redox (pseudocapacitive) behaviour of the

cobalt molybdate. This also confirms the rates of electronic and ionic transport are sufficient

enough to diffuse into the material and suitable for high rate applications. Among the samples

studied, the shape of the curve for nanospheres (Fig. 8e) is quasi-rectangular with a larger

area implying the capacitive behaviour which is mainly attributed to the carbon functional

group derived from the optimised surfactant content. The presence of carbon enhances the

electronic conductivity of the electrode and particles in good contact which enables the redox

mechanism. In the case of the other two samples, nanorods (Fig. 8d) and nanoneedles (Fig.

8f) exhibit an elliptical shape implying the materials are not readily reversible which supports

the galvanostatic studies showed in Fig. 10A. The differences shown in the physico-chemical

characterization explains the meagre performance of the nanorods and nanoneedles.

Electrochemical impedance spectroscopy (EIS) measurements were carried out for all the

three $CoMoO_4$ samples and the results are compared in Fig. S3, ESI§. Impedance analysis is

a strong tool to study the conductivity of the $CoMoO_4$ samples. From the Nyquist plots, at the

high frequency region, the point intersecting on the real axis represents the equivalent series

resistance (ESR), representing the resistance caused by the transfer of ions across the

electrode/electrolyte interface. [35] ESR includes the ionic resistance of electrolyte, resistance

of active material and resistance between electrode and electrolyte. The ESR was recorded

10.7 Ω, 1.8 Ω and 35 Ω for nanorods, nanospheres and nanoneedles, respectively. This

suggests that a nanosphere has the lowest resistance among the samples studied which is a

prerequisite for the capacitor characteristics. Also, at a low frequency region, the Warburg

impedance for nanosphere is found to be lower than that of nanorods and nanoneedles. The

indicator is the straight line closer to 90° at the lower frequency region is a representation for

an ideal supercapacitor. [11] This specifies the fact that the nanosphere led to reduce the mass

transfer resistance and improves the diffusion of ion in the electrode material. This is in

agreement with the results of physical characterisation discussed in the earlier section 2.1.

The Nyquist plots of $CoMoO_4$ materials are further analysed using Bode magnitude

and phase plots, shown in Fig. S4, ESI§. The qualitative analyses of the real (C′) and

imaginary (C″) capacitances are calculated using the following equations (6-7) [36].

$$C'(\omega) = -\frac{Z''(\omega)}{\omega \, |Z\omega|^2} \qquad \text{Eq.} \qquad (6)$$

$$C''(\omega) = -\frac{Z'(\omega)}{\omega \, |Z\omega|^2} \qquad \text{Eq.} \qquad (7)$$

where Z is complex impedance; Z′ and Z″ are real and imaginary part of the electrochemical

impedance respectively and ω represents the frequency. C′ represents the real (deliverable)

capacitance of the cell at the respective frequency, whereas C″ denotes the energy dissipated

in the device. [36] The frequency dependence of the capacitance plots are shown in Fig. S4 (A-

C). For all the samples studied, at lower frequencies, the observed capacitance is high but at

higher frequencies there was a sharp fall in capacity. This indicates the diffusion of ions from

the NaOH occurs deep inside the molybdates contributing to pseudocapacitive behaviour at

lower frequencies while the ions adsorb/desorb at higher frequencies leading to double layer

capacitive behavior. The high pseudocapacitive behaviour is observed for the $CoMoO_4$ with a

surfactant loading 1.0. The role of surfactant can be identified in the Bode plot showing

impedance versus frequency in Fig. S4 (D). The observed impedance is lower for surfactant

added sample implying the conductivity of this material has been improved and hence the

observed high capacitance. The typical behaviour of the material was also evident from the

Bode phase-angle plot shown in Fig. S4 (E). From the Bode plot, the observed maximum

phase angle is - 60°, a deviation from the ideal capacitor which is -90° [37] further supports the

pseudocapacitor behavior of the hybrid device. These results can be explained by the

pseudocapacitance, exhibited by the surfactant modified electrode of 1.0 loading.

2.2 *Effect of synthesis temperature in the presence of optimised F127 ratio on morphology and redox properties of synthesized $CoMoO_4$ nanospheres*

Evidently, $CoMoO_4$ material synthesised in the presence of F127 surfactant loading 1.0

showed promising electrochemical performance. There have been no studies widely reported

on the mechanism associated with the reaction temperature of precursors along with the

surfactant F127 to produce $CoMoO_4$. However, it's been reported that the physical characteristics of F127 is unique, the CMC and the surface activity depend on the synthesis temperature, to that of conventional surfactants.[23] To examine this, samples were synthesised at a range of temperature to investigate its effect on the morphology and redox behaviour in relation to their use in capacitors.

(a) Physicochemical Characterization

XRD patterns of $CoMoO_4$ material synthesised at reaction temperatures (300, 400 and 500 ^{o}C) are presented in Fig. 11. The XRD patterns show the evolution of peaks at a higher temperature. All the peaks are the characteristic diffraction peaks of $CoMoO_4$ material. At a higher temperature (500 ^{o}C in Fig. 11c) the diffraction peaks are getting sharper and narrow in width indicating the degree of crystallinity. The morphological analysis of the synthesised samples at various temperatures was performed using FESEM and TEM imaging. Fig. 12a-c demonstrates the typical FESEM images of the $CoMoO_4$ samples synthesized at 300, 400 and 500 ^{o}C. As seen in Fig. 12a-c, all the $CoMoO_4$ products are composed of spherical shaped nanoparticles but with an increasing particle size. At a higher reaction temperatures (>300 ^{o}C in Fig. 12b-c), particles tend to aggregate to form hierarchical spherical shaped [24] particle while eliminating the available pores. The diameter of the individual spherical particle increased from 1 μm to few μm resulting in a microsphere at higher temperature. The increase in reaction temperature may disintegrate the structured water surrounding the hydrophobic interactions among the chains in F127 surfactant. This could disfavour the micellar formation and the template may become inactive resulting in the formation of microspheres. It's also been reported that the effective volume fraction of the micelles decreases with the increasing reaction temperature. [23] The individual nanoparticles may agglomerate during the synthesis and the particle size will become large. [22] The microspheres may have limited access to the pores which could have resulted in less ion diffusion and

lower capacitance. Fig. 12d-f shows a corresponding TEM images. In parallel to FESEM, the TEM images confirm the spherical shaped morphology of rigid, less porous in nature of the CoMoO$_4$ materials synthesized at the elevated temperature. Also, the dark contrast regions in Fig. 12e-f may correspond to twining and dislocations due to the stress that the material has undergone during the reaction temperature.[28-29] Based on the aforementioned observations, we can conclude that the crystallinity and the particle shape of the synthesized CoMoO$_4$ product can be regulated by the synthetic temperature with an effective surfactant loading. Through physicochemical studies, it was demonstrated that the shape and size of CoMoO$_4$ products were strongly dependent on surfactant loading and the reaction temperature. The increase in concentration of the surfactant decreases the CMC, [23] while inducing the shape transformation from nanorods to nanospheres. On the other hand, the increase in temperature may disrupt the micellar formation and the template to control the pore size and distribution becomes ineffective.

In order to understand the role of pores in the synthesized CoMoO$_4$ at reaction temperatures (300, 400 and 500 ^{o}C), the nitrogen absorption-desorption isotherms and pore size distributions of CoMoO$_4$ samples were carried out and the plots are shown in Fig. S5, ESI§. The observed Type IV isotherm and BJH plot for the samples indicate that synthesised CoMoO$_4$ materials are mesoporous. Although the isotherms appear to be quite similar at various temperatures but a significant change in surface area has been observed among them. The BET surface area of 21 m^2 g^{-1} was obtained for 300° C sample while the surface area remains the same for 400° C but it decreased significantly to 13 m^2 g^{-1} for 500° C. The results of BET studies further confirm the fact that average particle size of the samples increases from 280 nm to 460 nm upon increasing the synthesis temperature from 300 ^{o}C to 500 ^{o}C. It could be tied to the fact that small individual particles tend to be fused together and

agglomerated in clusters at higher temperatures favouring the Ostwald ripening theory as

observed in Fig. 12.

(b) Electrochemical Characterization

To evaluate the redox properties of the $CoMoO_4$ material synthesised at various synthesis

temperatures, cyclic voltammetric studies were carried out using a standard three electrode

system in 2 M NaOH solution. Fig. 13a-c show the cyclic voltammetric profiles for the

repeated cycles of the samples synthesized at 300, 400 and 500 ^{o}C respectively at a scan rate

of 1 mV s^{-1} in the potential region 0.0 to 0.7 V. As the synthesis temperature increases, the

integral area under the peaks decreases implying the material is becoming electrochemically

less active. For the same mass loading, the CV profile possessing different areas for material

synthesized at different temperatures, indicates different levels of energy has been stored.

Nevertheless, a pair of redox peaks observed during the anodic and cathodic potential

suggests that the charge storage arises from the redox reaction of Co^{2+}/Co^{3+}. [11] The well-

defined peaks observed for 300 and 400 ^{o}C (compared in Fig. 13d) indicate that the materials

synthesized at lower temperatures exhibited a potential for high capacitance value. [8] A very

similar trend has been observed from galvanostatic measurements (Fig. 14 a - c) showing

superior characteristics for 300 and 400 ^{o}C samples with reversible specific capacitances of

204 and 200 F g^{-1}, respectively at a lower current density of 0.1 A g^{-1}. In the case of 500 ^{o}C, a

lower specific capacitance of 175 F g^{-1} has been achieved at a current density of 0.1 A g^{-1}. At

a higher current density of 1 A g^{-1}, only a very small capacitance of 15 F g^{-1} could be derived

implying the material synthesized at 500 ^{o}C may not be suitable for high power applications.

The characteristic charge-discharge profiles of the $CoMoO_4$ material synthesised at

various synthesis temperatures can also be found in Fig. 15A. Among the three samples

studied, material synthesised at 300 ^{o}C showed higher initial capacitance value of 79 F g^{-1}

with only a marginal difference seen for 400 ^{o}C exhibiting 75 F g^{-1}. On the other hand, the

500 ^{o}C showed relatively a lower specific capacitance of 60 F g^{-1}. The variation in particle size and the surface area explains the difference seen in the capacitance. The deviation from the typical triangular (charge-discharge) curve illustrates a typical faradaic reactions occurring at the electrode / electrolyte interface (peak C2 in the Fig. 13) and a non-faradaic reaction occurring at the surface by the adsorption of OH$^-$ ions (peak C1 in the Fig. 13) totalling a capacitance of 79 F g^{-1} resulting from the hybrid device. These factors are contributed to the enhanced storage level of capacitance. Moreover, the charge-discharge results are further corroborated from the cyclic voltammetric profiles shown in Fig. 14 (d – f). A broad quasi-rectangular shaped box like area is identified for 300 and 400 ^{o}C samples as seen in Fig. 14 (d - e) whereas a narrow shaped profile, with the absence of reduction peak C2 and in contrast to those of quasi-rectangular shape, is viewed for 500 ^{o}C sample in Fig. 14 (f). This is due to the fact that the material synthesised at 500 ^{o}C resulted in a lower surface area having microtwinning and dislocations which inhibited the access of active sites of the electrode. For 300 and 400 ^{o}C samples, increased current with increase in scan rates from 1 to 10 mV s^{-1} reveal an excellent high rate performances. All these results suggested that the lower synthesis temperature with optimised surfactant content was stable for supercapacitor electrode material.

The longevity of electrode materials is another important requirement for practical applications. Figure 15B shows the profile for specific capacitances vs. cycle number, which revealed that with the increase in reaction temperature there is a significant drop in retention after 2000 cycles for the samples synthesized at higher temperatures losing 60% of its initial capacitance. However, all the devices are reversible and 300 ^{o}C sample showed superior characteristics among the samples studied. The specific capacitance decreased slightly up to few cycles and then tended to stabilise. Table 2 summarises the capacitance values of the 1st and 2000th cycles and its energy density of CoMoO$_4$ samples synthesised at different

temperatures. The observed specific capacitance and energy density are comparable to that of the $CoMoO_4$ reported for hybrid device in aqueous solutions. [11, 20, 38]

The Nyquist plots for $CoMoO_4$ materials synthesised at different temperatures measured by electrochemical impedance spectroscopy (EIS) are shown in Fig. S6, ESI§. A semicircle at the high frequency region was observed for all three samples. The diameter of the semicircle is a representative of the charge transfer resistance (R_{ct}). The measured charge transfer resistance was 10 Ω, 14 Ω and 28 Ω for the samples, 300, 400 and 500 ^{o}C respectively. The lower R_{ct} values indicate faster charge-discharge ability. [11] In addition, ESR values were increased with increasing the synthesis temperature of $CoMoO_4$ materials. The ESR values of 1.79 Ω, 2.1 Ω and 2.3 Ω, respectively. The frequency dependence of the capacitance plots shown in Fig S7, ESI§ (A-C) denotes the observed capacitance is higher for the sample synthesized at temperature 300 ^{o}C. The Bode plots (Fig. S7 D) and phase angle (Fig. S7 E) also support the fact that $CoMoO_4$ synthesized at a lower temperature favours for a pseudocapacitance behaviour. This confirms the 300 ^{o}C sample possess better conductivity, pore size distribution and hence the high specific capacitance and its retention after multiple cycles.

3. Experimental

3.1 Synthesis of CoMoO4 Materials

Three cobalt molybdate ($CoMoO_4$) samples were synthesised using analytically pure $Co(NO_3)_2.6H_2O$ (6.648 g) and $(NH_4)_6Mo_7O_{24}.4H_2O$ (4.033 g) with variable amount of non-ionic Pluronic F127 surfactant known as F127 of Mw = 12600, all chemicals supplied by Sigma Aldrich. The metal and molybdate reactants were dissolved in 20 mL of de-ionised water at 80 ^{o}C with an effective stirring to obtain a homogenous solution. Then, the required amount (0.8, 1.7 and 2.5 g) of F127 was added in the bath, while maintaining the cobalt to surfactant ratio 1:0.5, 1:1 and 1:2. The pH of the solution was adjusted by drop wise addition

of ammonia solution. Subsequently, the mixture was dried at 150 ^{o}C in hot air oven for 12 h. Later, the dried mass was transferred into a furnace heating. $CoMoO_4$ material was synthesised at 300 ^{o}C for 3 hours with different surfactant loadings 0.8, 1.7 and 2.5 g of F127 labelled as "0.5", "1.0" and "2.0", respectively. The critical micelle concentration for F127 was found to be 1.27 g above which micelles are formed in the solutions.[23]

When the metal to surfactant ratio was optimised, for the second part of the study, the best performed $CoMoO_4$ material was further examined to evaluate the effect of the synthesis temperature on the supercapacitive performance. Samples were synthesised at a range of temperatures 300, 400 and 500 ^{o}C and the other conditions were kept identical. For comparison purposes, $CoMoO_4$ material in the absence of F127 surfactant was also synthesised and examined.

3.2. Physical characterisation

The materials synthesised were characterized extensively by physical and electrochemical techniques. X-ray diffraction (XRD) was used to identify the crystal structure of synthesized $CoMoO_4$ product using Siemens D500 X-ray diffractometer 5635 with a Cu kα source at a scan speed of 1° min^{-1}. The voltage and current were 38 kV and 28 mA, respectively. A high magnification Zeiss Neon 40ESB Field Emission Scanning Electron Microscope (FESEM) instrument was also used to acquire morphological and microstructure information of samples. The nanostructure and lattice imaging of the $CoMoO_4$ materials was characterised by transmission electron microscopy (TEM) and high-resolution TEM, using a JEOL 200F TEM operated at 200 kV. TEM specimens were prepared by grinding a small amount of powder under methanol and dispersing on a holey carbon film. Pore structures and surface area of the samples were characterized by nitrogen adsorption/ desorption Micromeritics Tristar II Surface area and porosity analyser. Before analysing, the $CoMoO_4$ samples were degassed at 100 °C overnight. To analyse the mechanism involved in the $CoMoO_4$, surface

study for all surfactant ratios were made using X-ray photoelectron spectroscope (XPS) with monochromatic Al Kα (1486.6 eV) radiation. Carbon (1s) was used as a reference for all samples. The XPS data were analysed using Casa XPS software and the necessary curve fits are made.

3.3 Electrochemical Characterisation

For electrochemical measurement, the electrode was prepared by mixing $CoMoO_4$ (75 wt. %), carbon black (15 wt. %) and PVDF (10 wt. %) with 0.4 mL of NMP to make slurry. This was coated on a small piece of carbon sheet (area of coating, 1 cm^2). The remainder of the carbon strip was masked using an insulation film to obtain a coated surface area of 1 cm^2 exposed to the aqueous (NaOH) electrolyte. The loaded active material was 15 mg in each case. To prepare the active negative electrode material, activated carbon (AC) (90 wt. %) and PVDF (10 wt. %) were used. A full cell termed as "hybrid device" (AC‖$CoMoO_4$) was fabricated by using polypropylene separator. The cyclic voltammetry and galvanostatic charge-discharge studies of the composites were carried out using SP-150, Bio-Logic Science Instruments in 2 M NaOH electrolyte at room temperature. The ionic conductivity of aqueous solution is two orders of magnitude greater than that of organic electrolytes, allowing higher discharge rates and lower voltage drops due to electrolyte impedance [14] which is discussed in section 2.1 under EIS spectroscopy.

For the three-electrode tests, a platinum wire of 10 cm length and 1 mm diameter in dimension and mercury–mercuric oxide (Hg/HgO) served as the counter and reference electrodes, respectively. $CoMoO_4$ served as the working electrode. Galvanostatic charge-discharge cycles (two electrode system) were performed using an 8-channel battery analyser from MTI Corp. USA. The cyclic voltammetric profiles were obtained for the hybrid device with various sweep rates ranging between 1 and 10 mV s^{-1}. Charge–discharge studies of the hybrid device were carried out at a current density of 0.2 A g^{-1}. The cut-off charge and

discharge voltages were 1.6 and 0 V, respectively. Charge – discharge measurements of the $CoMoO_4$ in a three electrode system were carried out at a range of current densities from 0.1 to 1 A g^{-1} within the voltage range between 0 and 0.6 V. Specific capacitance and energy density of the device were calculated at the end of each discharge. Electrochemical impedance spectroscopy (EIS) and bode plots were carried out with amplitude of 5 mV over a frequency range of 10 mHz to 700 KHz at open circuit potential. The optimal mass ratio between the two electrodes, AC and $CoMoO_4$, was determined to be 1.6 for the fabricated hybrid capacitor. Therefore, the mass of the AC (negative) and $CoMoO_4$ (positive) electrode was 24.0 and 15.0 mg, respectively.

Conclusions

The present study provides new insights on tuning the redox properties of $CoMoO_4$ through shape control of morphologies from nanospheres to nanorods and nanoneedles varying the concentration of F127 surfactant. The specific capacitance and cycling stability of $CoMoO_4$ materials was found to be significantly dependent on the morphology and structure of the materials. The correlation between the redox behaviour of cobalt and the shape control effects of surfactant loadings were established. With the variation of metal to surfactant ratio, 1:1 exhibited a well-defined redox peak of high specific capacitance 79 F g^{-1} retaining 75 % of its initial value. This excellent electrochemical performance is attributed to the unique nanospheres having individual hexagonal shaped particles. The available high surface area of the sample is driven from the micellar formation of F127 surfactant. Our physicochemical and electrochemical results showed that $CoMoO_4$ synthesized at elevated temperature (> 400 ^{o}C) does not found to be suitable for energy storage applications. The high surface area and short ion diffusion path make the $CoMoO_4$ sample synthesised at 300 ^{o}C at the optimised ratio of 1.0 surfactant loading to exhibit specific capacitance of 79 F g^{-1} with excellent

cycling stability. The results of the hybrid capacitor ($CoMoO_4$ vs. AC) show through tuning the redox properties it has a potential to store renewable energy.

Acknowledgments

References

1. Umashankar, M.; Palaniappan, S. Hybrid composite of nitrogen functionalised graphene-polyanilline electrode for high performance supercapacitor. *RSC Adv.* **2015,** 5, 70657-70681.

2. Salunkhe, R. R.; Tang, J.; Kamachi, Y.; Nakato, T.; Kim, J. H.; Yamauchi, Y. Asymmetric supercapacitors using 3D nanoporous carbon and cobalt oxide electrodes synthesized from a single metal–organic framework. *ACS Nano*, **2015**, *9*, 6288-6296.

3. Tang, J.; Liu, J.; Torad, N. L.; Kimura, T.; Yamauchi, Y. Tailored design of functional nanoporous carbon materials toward fuel cell applications. *Nano Today*, **2014**, 9, 305-323.

4. Torad, N. L.; Salunkhe, R. R.; Li, Y.; Hamoudi, H.; Imura, M.; Sakka, Y.; Hu, C. – C.; Yamauchi, Y. Electric double-layer capacitors based on highly graphitized nanoporous carbons derived from ZIF-67. *Chem. Euro. J*, **2014**, 20, 7895-7900.

5. Lokhande, C. D.; Dubal, D. P.; Joo, O. S. Metal Oxide thin film based supercapacitors. *Curr. Appl. Phy.* **2011**, 11, 255 - 270.

6. Bao, F.; Zhang, Z.; Guo, W.; Liu, X. Facile syntheisis of three dimentional $NiCo_2O_4$@MnO_2 core shell nanosheet array and its supercapacitive performance. *Electrochim. Acta* **2015,** 157, 31-40.

7. Minakshi, M.; Meyrick, D.; Appadoo, D. Maricite (NaMn$_{1/3}$Ni$_{1/3}$Co$_{1/3}$PO$_4$)/Activated Carbon: Hybrid Capacitor. *Energy & Fuels* **2013**, 27, 3516 - 3522.

8. Hu, X.; Zhang, W.; Liu, X.; Mei, Y.; Huang, Y. Nanostructured Mo-based electrode materials for electrochemical energy storage. *Chem. Soc. Rev.* **2015**, 44, 2376 - 2404.

9. Mai, L. Q.; Yang, F.; Zhao, Y. L.; Xu, X.; Xu, L.; Luo, Y. Z. Hierarchical MnMoO$_4$/CoMoO$_4$ hetrostructured nanowires with enhanced supercapacitorr performance. *Nat. Commun.* **2011,** 2, 381-385.

10. Mandal, M.; Ghosh, D.; Giri, S.; Shakir, I.; Das, C. Polyaniline-wrapped 1D CoMoO$_4$. 0.75 H$_2$O nanorods as electrode material for dupercapacitor energy storage applications. *RSC Adv.* **2014,** 4, 30832-30839.

11. Ramkumar, R.; Minakshi, M. Fabrication of ultrathin CoMoO$_4$ nanosheets modified with chitosan and their improved performance in energy storage device. *Dalton Trans.* **2015,** 44, 6158-6168.

12. Cui, C.; Xu, J.; Wang, L.; Guo, D.; Mao, M.; Ma, J.; Wang, T. Growth of NiCo$_2$O$_4$@MnMoO$_4$ nanocolumn arrays with superior pseudocapacitor properties. *ACS Appl. Mater. Interfaces*, **2016**, 8, 8568-8575.

13. Veerasubramani, G.; Krishnamoorthy, K.; Kim, S. -J. Electrochemical performance of an asymmetric supercapacitor based on graphene and cobalt molybdate electrodes. *RSC Adv.*, **2015**, 5, 16319-16327.

14. Barmi, M.; Minakshi, M. Role of polymeric surfactant in the synthesis of cobalt molybdate nanospheres for hybrid capacitor applications. *RSC Adv.* **2016,** 6, 36152-36162.

15. Peng, S. J.; Li, L. L.; Wu, H. B.; Madhavi, S.; Lou, X. -W. Controlled Growth of NiMoO$_4$ Nanosheet and Nanorod Arrays on Various Conductive Substrates as Advanced Electrodes for Asymmetric Supercapacitors. *Adv. Energy Mater.* **2015**, 5, 1401172.

16. Jothi, P. R..; Shanthi, K.; Salunkhe, R. R.; Pramanik, M.; Malgras, V.; Alshehri, S. A.; Yamauchi, Y. Syntheisis and Charachterisation of α-NiMnO$_4$ nanorods for supercapacitor application. *European J. Inorg. Chem.* **2015**, 22, 3694-3699.

17. Senthilkumar, B.; Kalai Selvan, R. Hydrothermal synthesis and electrochemical performances of 1.7 V NiMoO$_4$xH$_2$O||FeMoO$_4$ aqueous hybrid supercapacitor. *J. Colloid Interface Sci.* **2014,** 426, 280-286.

18. Ding, Y.; Xia, C. F.; Zhou, H.; Wang, L.; Hu, X. L. Influence of sintering temperature on the structural and morphological performance of CoMoO$_4$. *Russian J. .Inorg. Chem.* **2012,** 57, 569-573.

19. Liu, M. C.; Kong, L. B.; Ma, X. J.; Lu, C.; Li, X. M.; Luo, Y. C.; Kang, L. Hydrothermal process for the fabrication of CoMoO$_4$. 0.9 H$_2$O nanorods with excellent electrochemical behaviour. *New J Chem.* **2012,** 36, 1713-1716.

20. Baskar, S.; Meyrick, D.; Kalai Sevlan, R.; Minakshi, M. Facile and large scale combustion synthesis of α-CoMoO$_4$: Mimics the redox behaviour of a battery in aqueous hybrid device. *Chem Eng. J.* **2014,** 253, 502-207.

21. Biswal, A.; Tripathy, B. C.; Li, D.; Minakshi, M. Electrodeposition of Pluronic F127 assisted rod-like EMD/carbon arrays for efficient energy storage. *Dalton Trans.* **2015,** 44, 16446-16457.

22. Lazaro, A.; Van de Griend, M. C.; Brouwers, H.; Geus, J. W. The influence of process conditions and ostwald ripening on the specific surface area of olivine nano-silica. *Microporous and Mesoporous Mater*. **2013**, 181, 254 - 261.

23. Wanka, G.; Hoffman, H.; Ulbricht, W. Phase diagrams and aggregation behaviour of Poly(oxyethylene) - Poly(oxypropylene) - Poly(oxyethylene) triblock coploymers in aqueous solutions. *Macromolecules* **1994**, 27, 4145 - 4159.

24. Mortensen, K. Phase behaviour of Poly(ethylene oxide) - Poly(proylene oxide) - Poly (ethylene oxide) triblock-copolymer dissolved in water. Europhys. Lett. **1992**, 19, 599 -604.

25. Bakshi, M. S. How surfactants control crystal growth of nanomaterials. *Cryst. Growth Des.* **2016**, 16, 1104 - 1133.

26. Cai, D.; Wang, D.; Liu, B.; Wang, Y.; Liu, Y.; Wang, L.; Li, H.; Huang, H.; Li, Q.; Wang, T. Comparison of the electrochemical performance of $NiMoO_4$ nanorods and hierarchical nanospheres for supercpacitor applications. *ACS Appl. Mater. Interfaces* **2013**, *5*, 12905 - 12910.

27. Xu, F.; Cai, R.; Zeng, Q.; Zou, C.; Wu, D.; Li, F.; Lu, X.; Liang, Y., Fu, R. Fast ion transport and high capacitance of polystryene-based hierarchical porous carbon electrode material for supercpacitors. *J. Mater. Chem.A* **2011**, 21, 1970 - 1976.

28. Yan, D.; Yan, P.; Cheng, S.; Chen, J.; Zhuo, R.; Feng, J.; Zhang, G. Fabrication, in-dpeth characterization, and formation mechanism of crystalline porous birnessite MnO_2 film with amorphous bottom layers by hydrothermal method. *Crys. Growth. Des.* **2009**, 9, 218 - 222.

29. Wu, G.; Zaefferer, S. Advances in TEM operation mircoscopy by combination of dark-field conical scanning and improved image matching. *Ultramicroscopy* **2009**, 109, 1317 - 1325.

30. Xia, X.; Lei, W.; Hao, Q.; Wang, W.; Wang, X. One-step synthesis of $CoMoO_4$/graphene composites with enhanced electrochemical properties for supercapacitors. *Electrochim. Acta* **2013**, 99, 253 - 261.

31. Ramkumar, R.; Minakshi, M. A biopolymer gel-decorated cobalt-molybdate nanowafer: effective graft polymer cross-linked with an organic acid for better energy storage. *New J. Chem.* **2016**, 40, 2863 - 2877.

32. Atuchin, V. V.; Khyzhun, O. Y.; Chimitova, O. D.; Molokeev, M. S.; Gavrilova, T. A.; Bazarov, B. G.; Bazarova, J. G. Electronic structure of β-RbNd(MoO$_4$)$_2$ by XPS and XES. *J. Phy. Chem. Solids* **2015**, 77, 101 - 108.

33. Chen, J.; Selloni, A. First principles study of cobalt (hydr)oxides under electrochemical conditions. *J. Phys. Chem. C* **2013**, 117, 20002 - 20006.

34. Yao, M.; Hu, Z.; Liu, Y.; Liu, P. A novel synthesis of size-controlled mesoporous NiMoO$_4$ nanospheres for supercapacitor applications. *Ionics* **2016**, 22, 701 - 709.

35. Wang, P.; Liu, H.; Xu, Y.; Chen, Y.; Yang, J.; Tan, Q. Supported ultrafine ruthenium oxides with specific capacitance up to 1099 F g^{-1} for a supercapacitor. *Electrochim. Acta.* **2016**, 194, 211 - 218.

36. Taberna, P. L.; Simon, P.; Fauvarque, J. F. Electrochemical characteristics and impedance spectroscopy studies of carbon-carbon supercapacitors, *J. Electrochemical Soc*. **2003**, 150, A292 - A300.

37. Arulepp, M.; Leis, J.; Latt, M.; Miller, F.; Rumma, K.; Lust, E.; Burke, A. The advanced carbide - derived carbon based supercapacitor. J. Power Sour. **2006**, 162, 1460 - 1466.

38. Cai, D.; Liu, B.; Wang, D.; Wang, L.; Liu, Y.; Li, H.; Wang, Y.; Li, Q.; Wang, T. Construction of unique NiCo$_2$O$_4$ nanowire@ CoMoO$_4$ nanoplate core/shell arrays on Ni foam for high areal capacitance supercapcitors. *J. Mater. Chem. A* **2014**, 2, 4954 - 4960.

Table 1 Transmission electron microscopy / energy dispersive spectral (TEM/EDS) analyses of CoMoO$_4$ at different locations (1 – 4) with typical elemental compositions

Surfactant loading 0.5	Co	Mo	O	Total wt. %
1	15.05	53.90	31.05	100.00
2	14.00	54.79	31.21	100.00
3	14.51	54.36	31.13	100.00
4	13.87	54.90	31.23	100.00
Surfactant loading 1.0	**Co**	**Mo**	**O**	**Total**
1	22.20	47.84	29.96	100.00
2	22.34	47.72	29.94	100.00
3	24.24	46.11	29.65	100.00
4	23.86	46.44	29.70	100.00

Table 2 Specific capacitance (SC) and energy density (E) of CoMoO$_4$ samples synthesised at (a) 300, (b) 400 and (c) 500°C in the presence of optimised surfactant loading 1.0.

Sample	Initial SC, F g^{-1}	SC, F g^{-1} after 2000 cycles	E, W h kg^{-1}
300 $^{\circ}$C	79	59	21
400 $^{\circ}$C	75	47	17
500 $^{\circ}$C	60	38	17
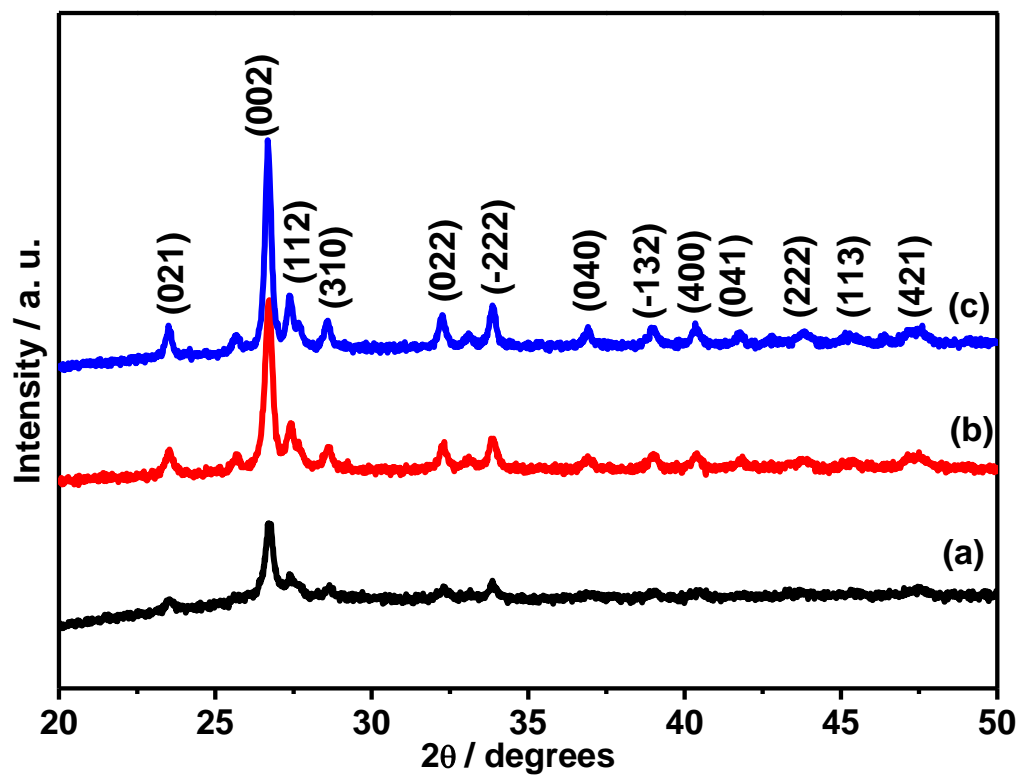
Figure 1 X-ray diffraction (XRD) patterns of $CoMoO_4$ synthesized with variable surfactant loadings (metal to surfactant ratios 1:0.5; 1:1; and 1:2) labelled as (a) 0.5, (b) 1.0 and (c) 2.0.
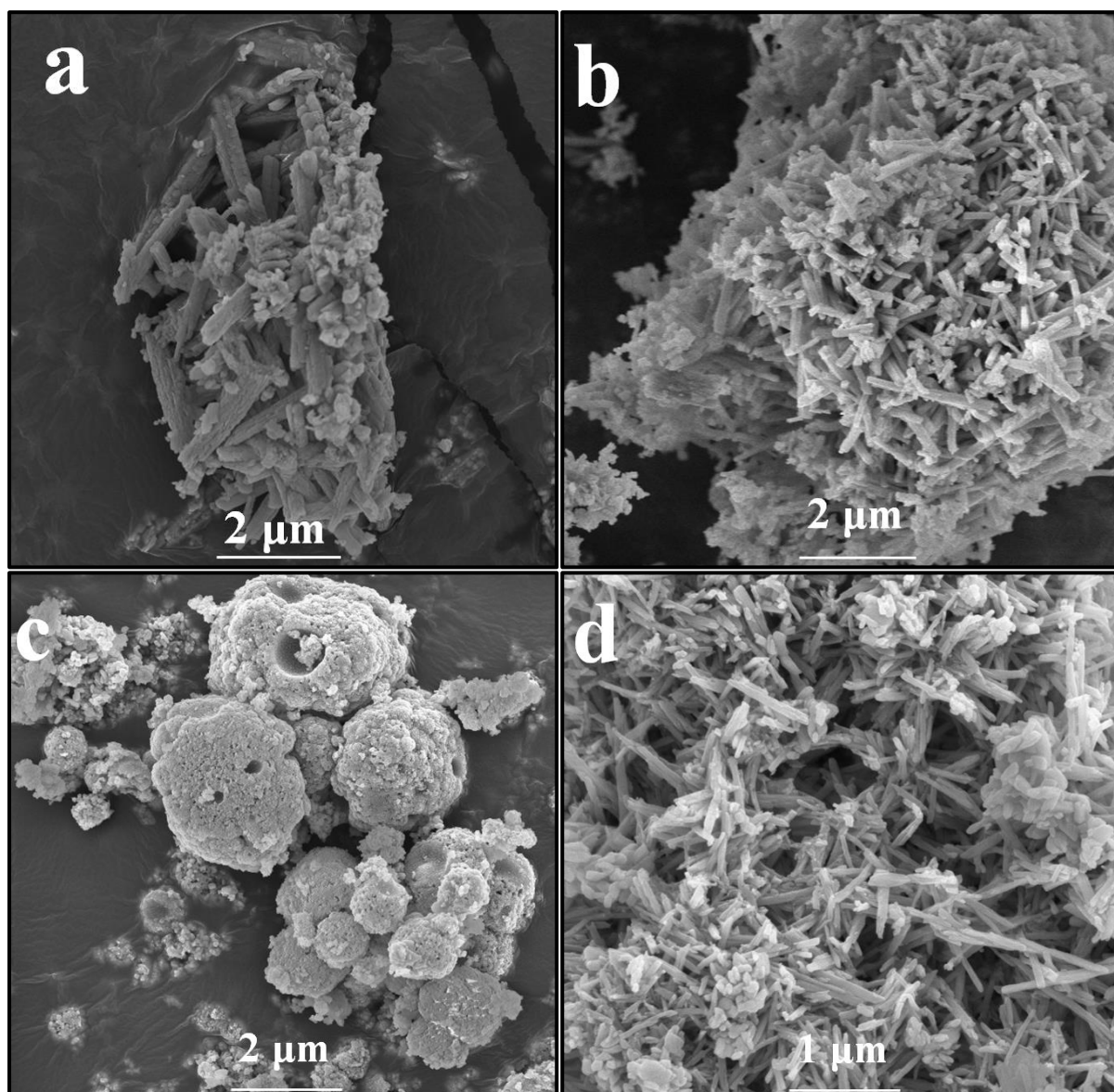
Figure 2 FE-SEM images of CoMoO$_4$ materials synthesized with a (a) surfactant – free

CoMoO$_4$ for a comparison, different surfactant loadings (metal to surfactant ratios 1:0.5; 1:1;

and 1:2) labelled as (b) 0.5, (c) 1.0 and (d) 2.0.
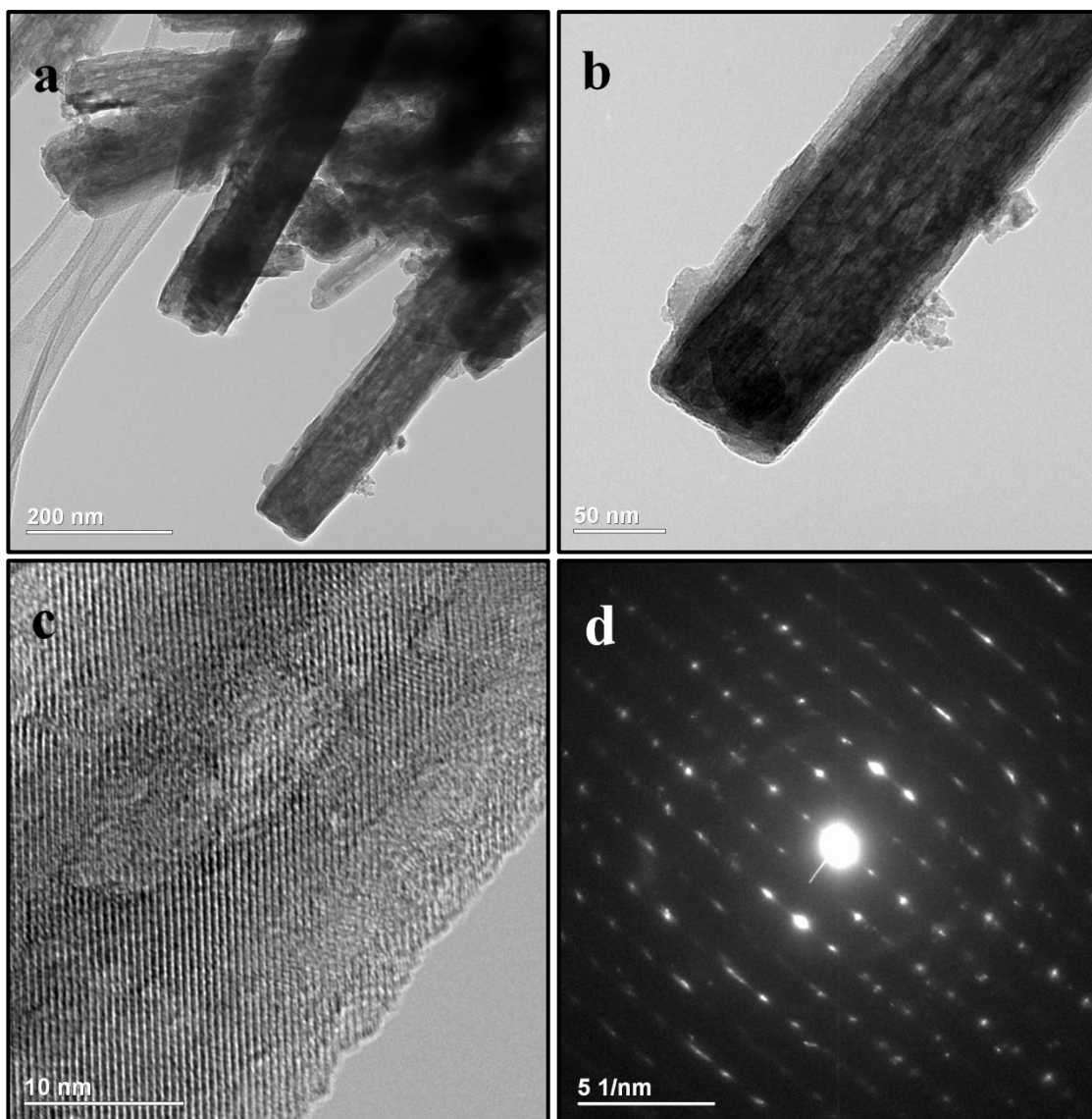
Figure 3 Transmission electron microscopy (TEM) images of CoMoO$_4$ materials with 0.5

loading. (a) Low and (b) high magnification TEM images, (c) high – resolsution HRTEM

imaging and (d) its selected area diffraction pattern (SADP) showing diffusive rings.
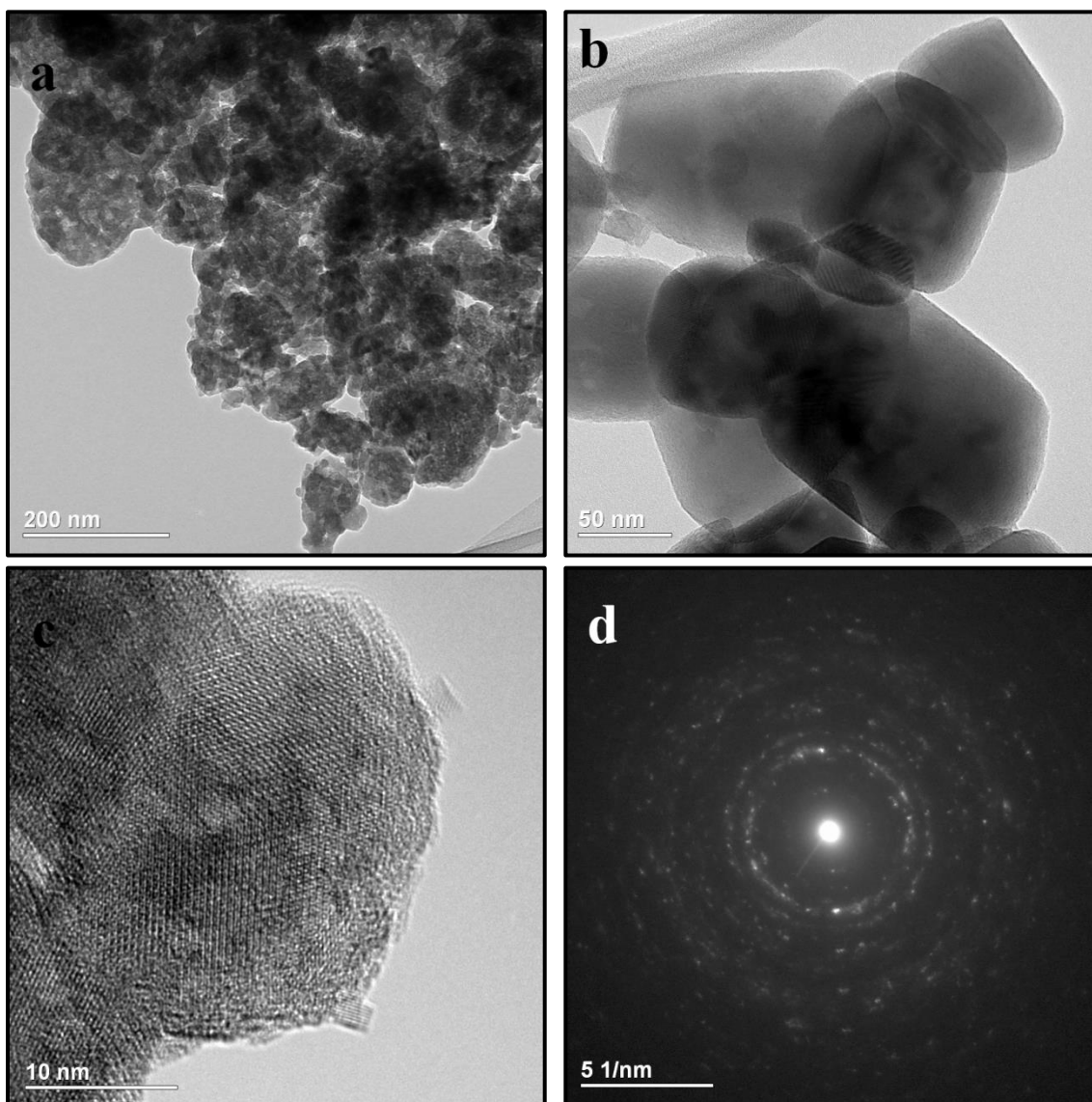
Figure 4 Transmission electron microscopy (TEM) images of CoMoO$_4$ materials with 1.0 loading. (a) Low and (b) high magnification TEM images showing hexagonal like crystallites, (c) high – resolsution HRTEM imaging and (d) its selected area diffraction pattern (SADP) showing well-defined rings.
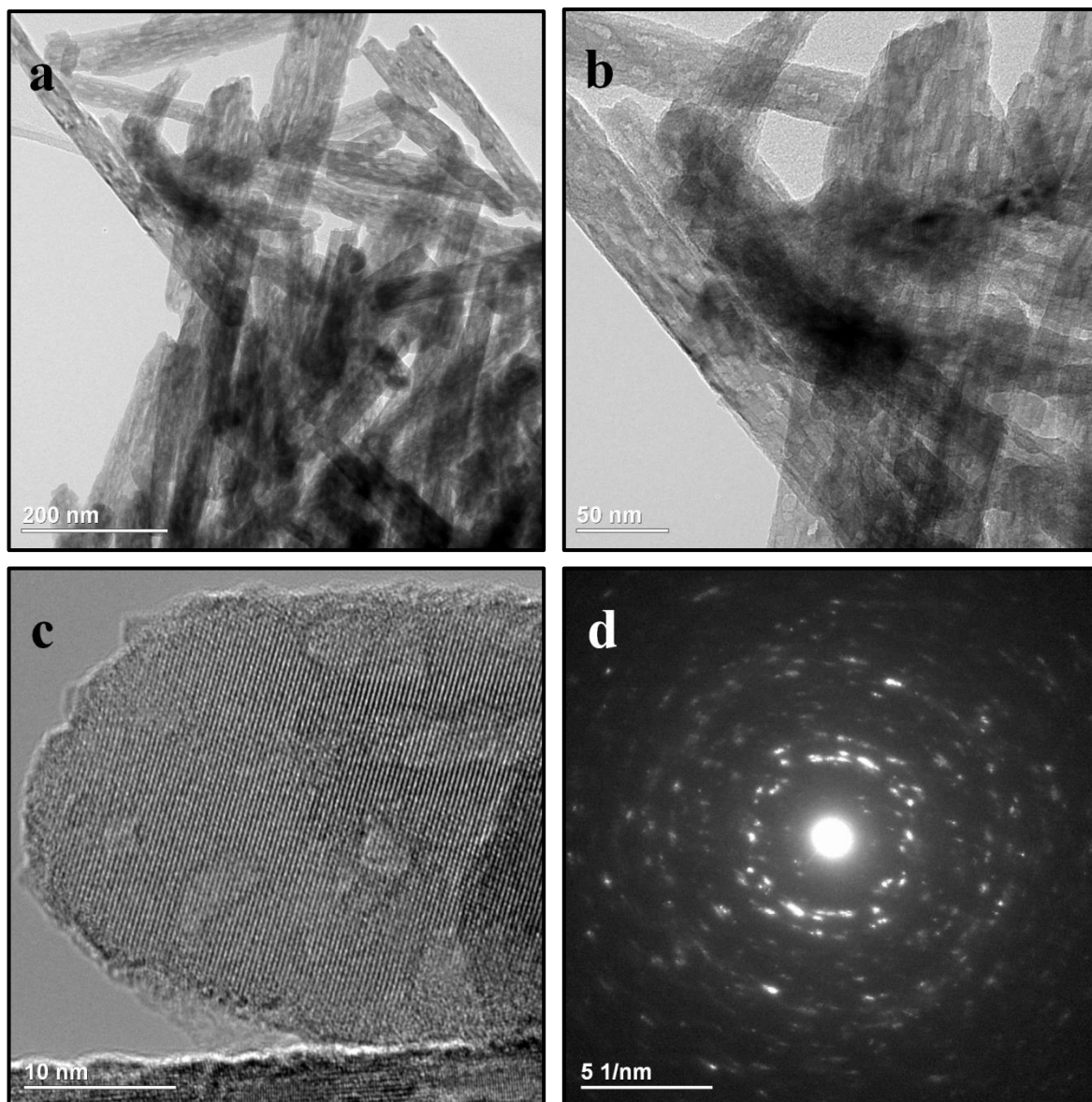
Figure 5 Transmission electron microscopy (TEM) images of CoMoO$_4$ materials with 2.0

loading. (a) Low and (b) high magnification TEM images showing microtwinning and

dislocations, (c) high – resolsution HRTEM imaging and (d) its selected area diffraction

pattern (SADP) showing polycrystalline characteristics.
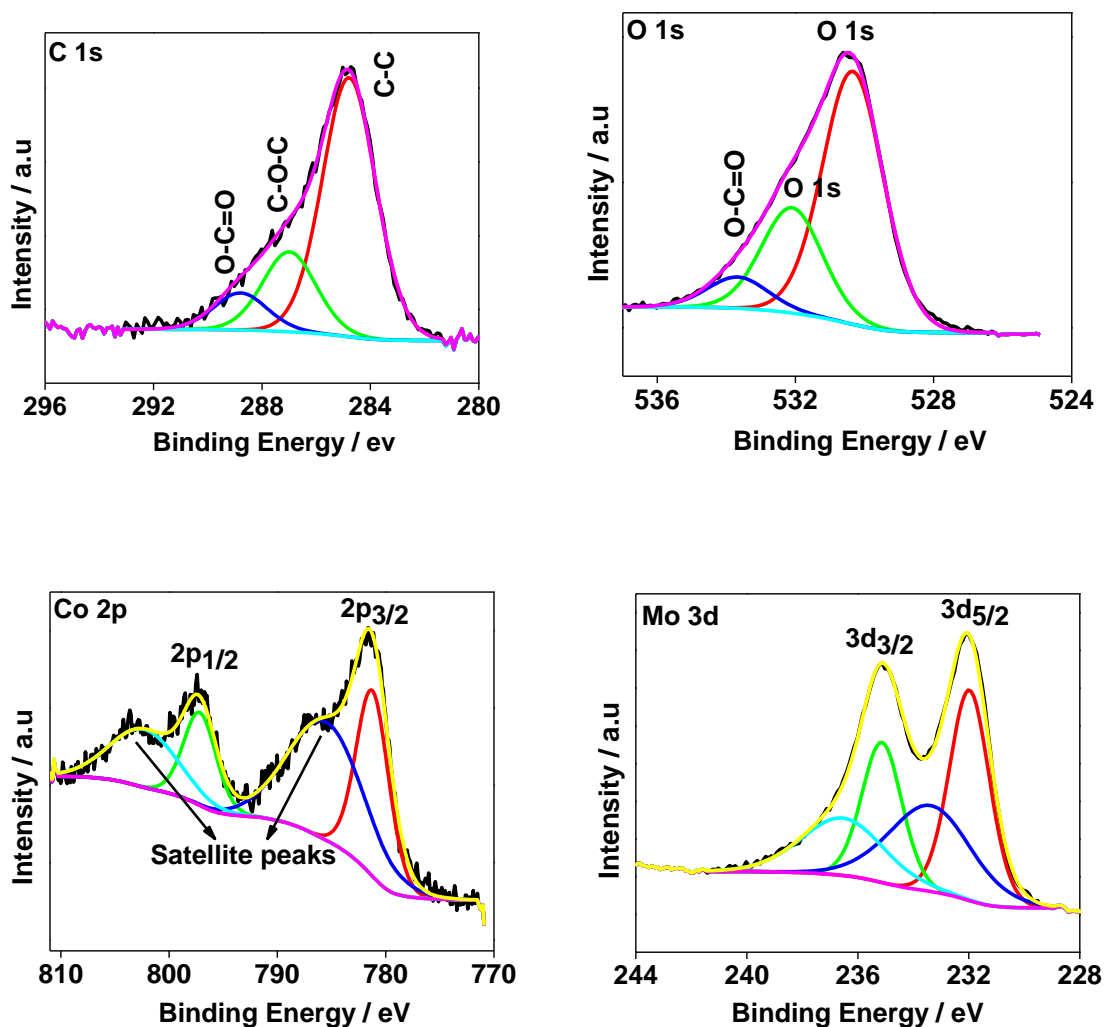
Figure 6 X-ray photoelectron spectroscopy (XPS) of C (1s), O (1s), Co (2p) and Mo (3d) for the CoMoO$_4$ material synthesized with a surfactant loading 0.5 ratio.
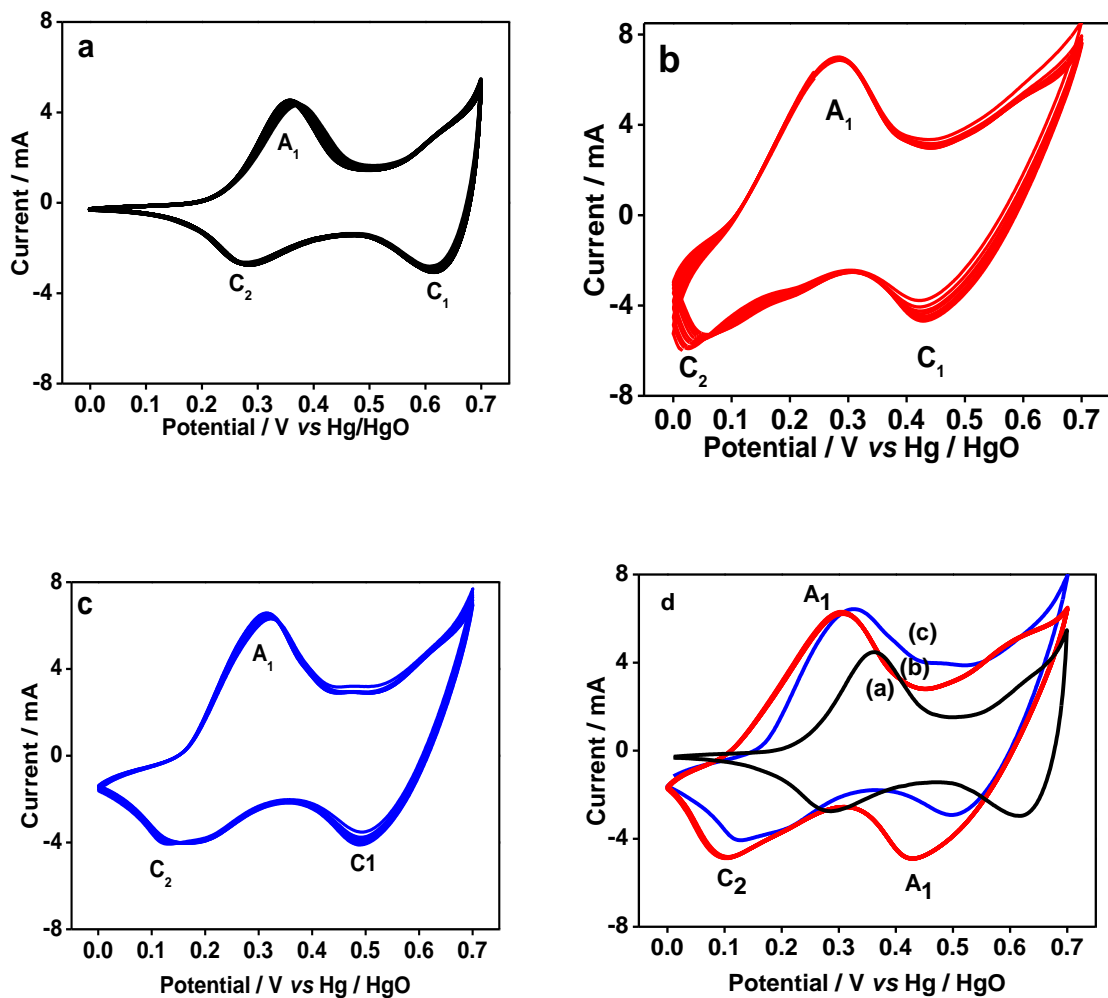
Figure 7 Cyclic voltammetric (CV) curves (three cell configuration) of CoMoO$_4$ materials synthesized at 300 ^{o}C with different surfactant loadings (a) 0.5, (b) 1.0 and (c) 2.0 showing data for multiple (50) cycling. (d) First CV curves are compared for three samples.
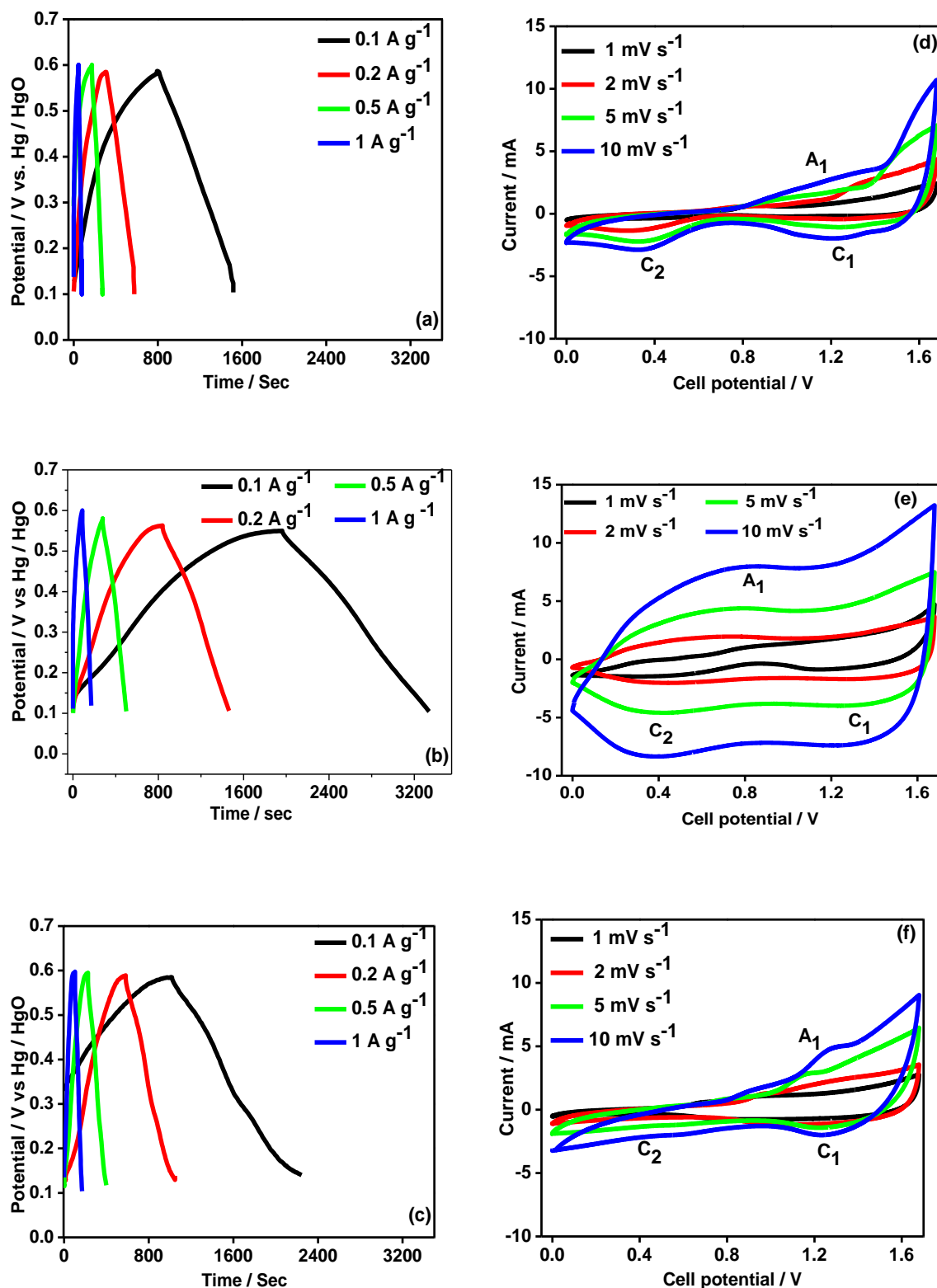
Fig. 8 (a – c) Charge – discharge behavior of $CoMoO_4$ (three cell configuration) electrodes and (d – f) cyclic voltammetric curves (CV; two cell configuration), oxidation – reduction behavior of hybrid capacitor AC ∥ $CoMoO_4$. The $CoMoO_4$ electrode synthesized at 300 °C with different surfactant loadings (a, d) 0.5, (b, e) 1.0 and (c, f) 2.0 are shown.
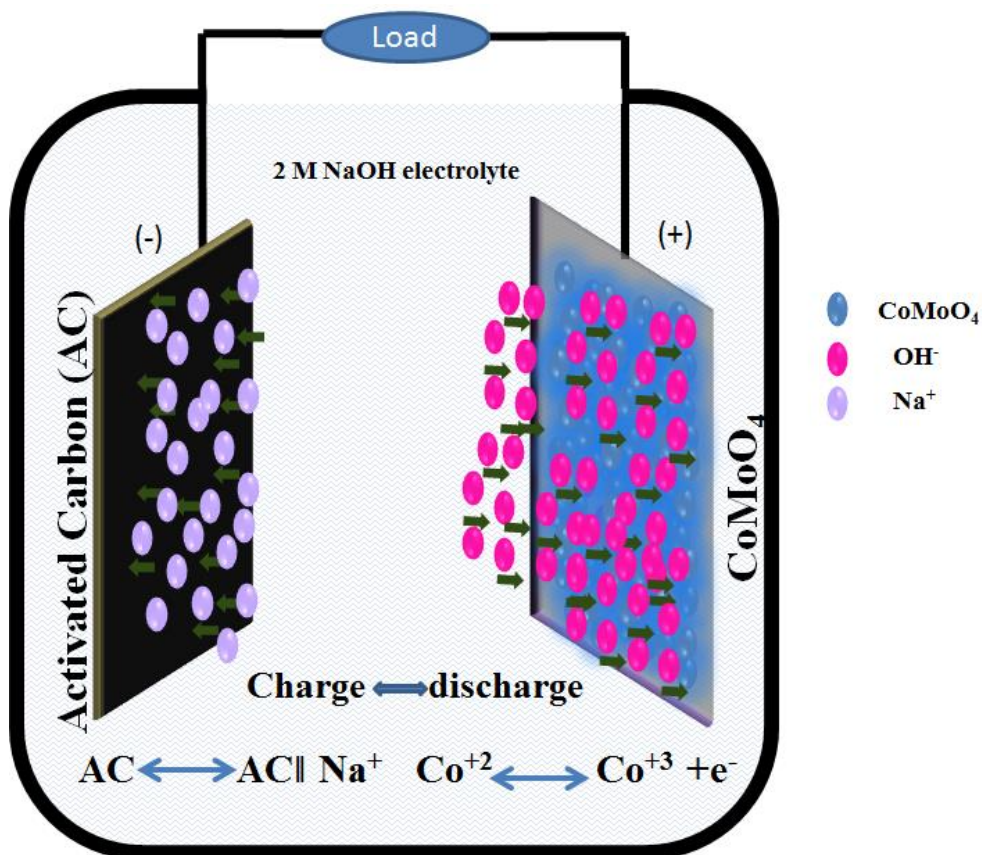
Figure 9 Schematic representation of asymmetric hybrid device used for electrochemical performance, $CoMoO_4$ is used as a cathode and activated carbon (AC) as an anode in 2 M NaOH electrolyte. Possible reactions are shown in the figure.
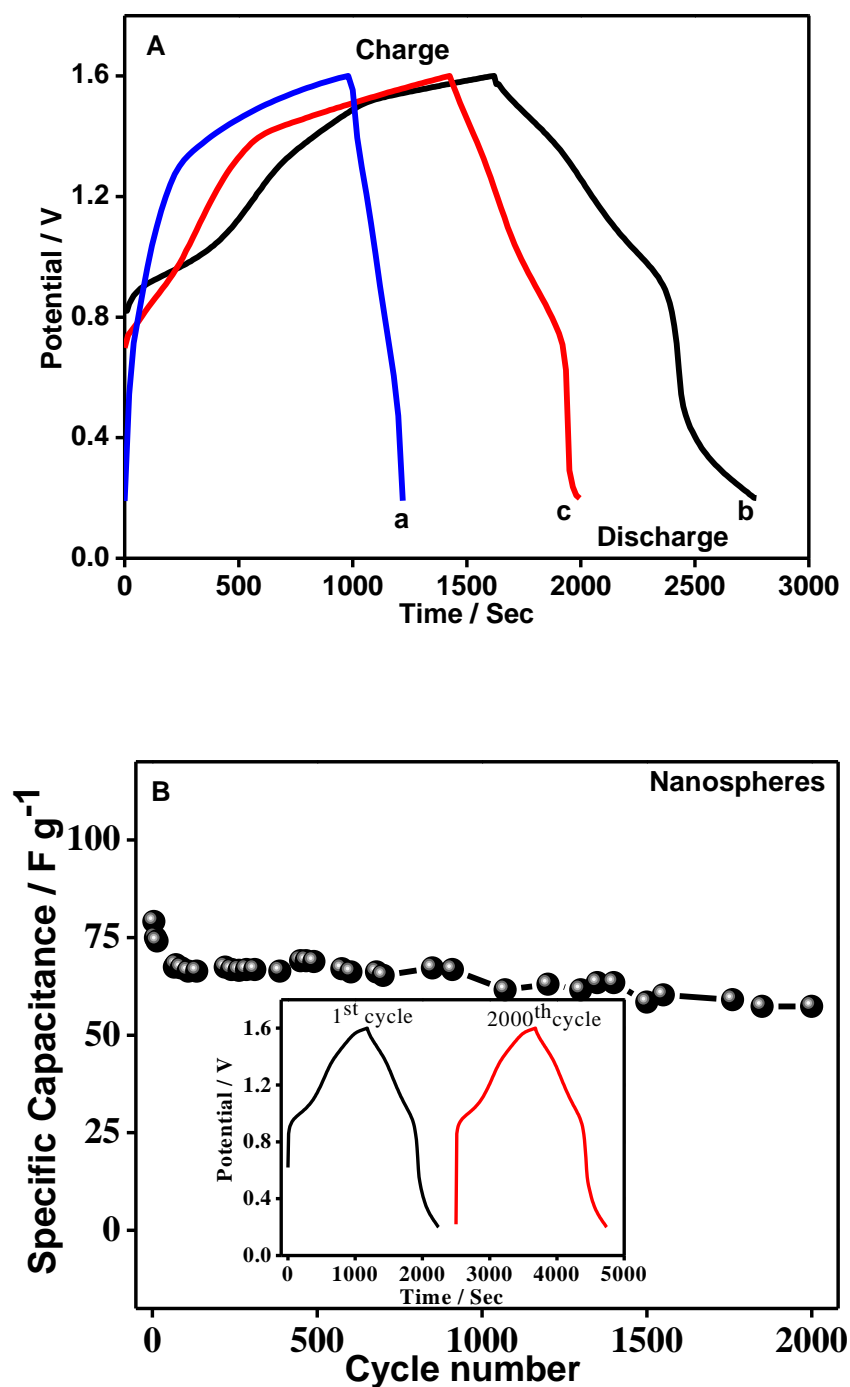
Figure 10 (A) Galvanostatic charge-discharge (two cell configuration) curves of CoMoO$_4$ materials synthesized at 300 $^{\circ}$C with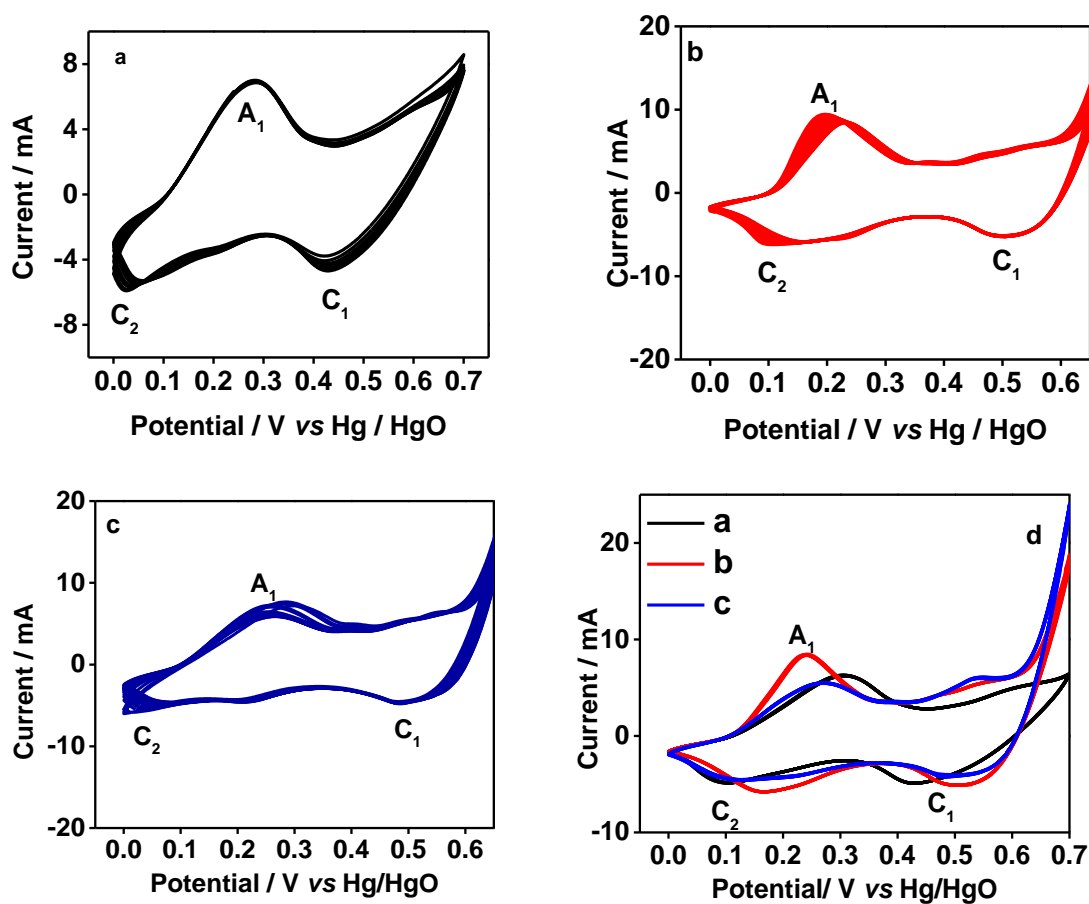 different surfactant loadings (a) 0.5, (b) 1.0 and (c) 2.0. (B) Variation of specific capacitance *vs.* cycle numbers for the best performed surfactant loading 1.0. Inset shows the charge-discharge profile for the first and 2000th cycle retaining its shape.
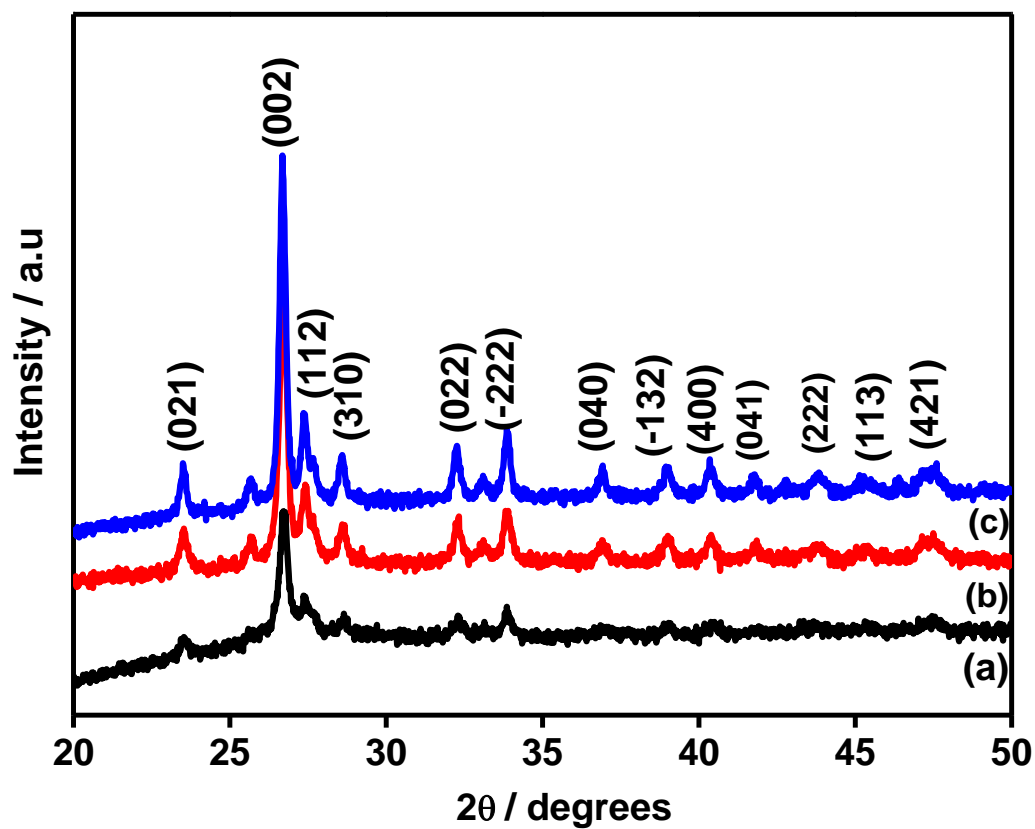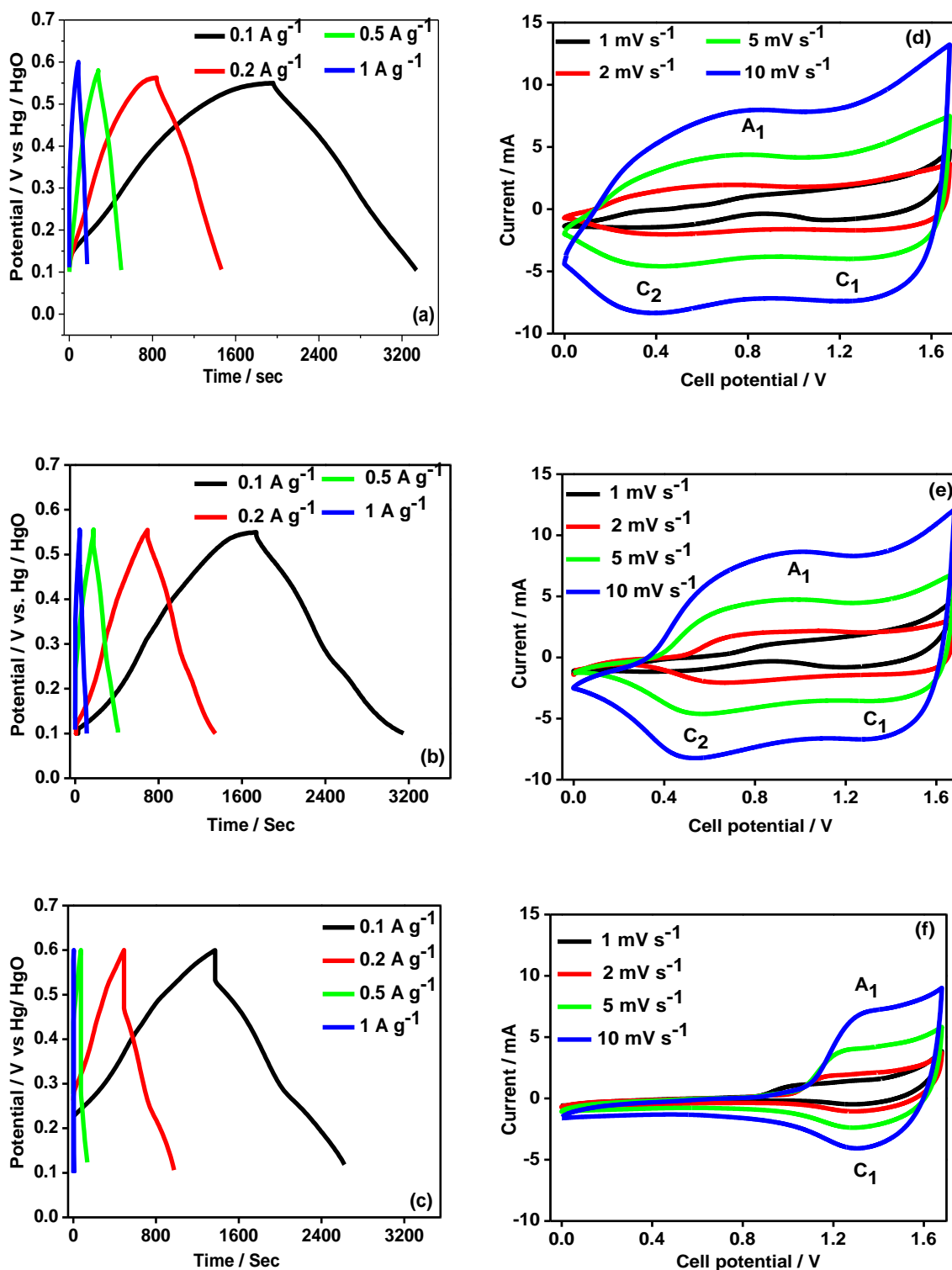
Figure 11 XRD patterns of CoMoO$_4$ materials synthesised at (a) 300, (b) 400 and (c) 500 $^{\circ}$C
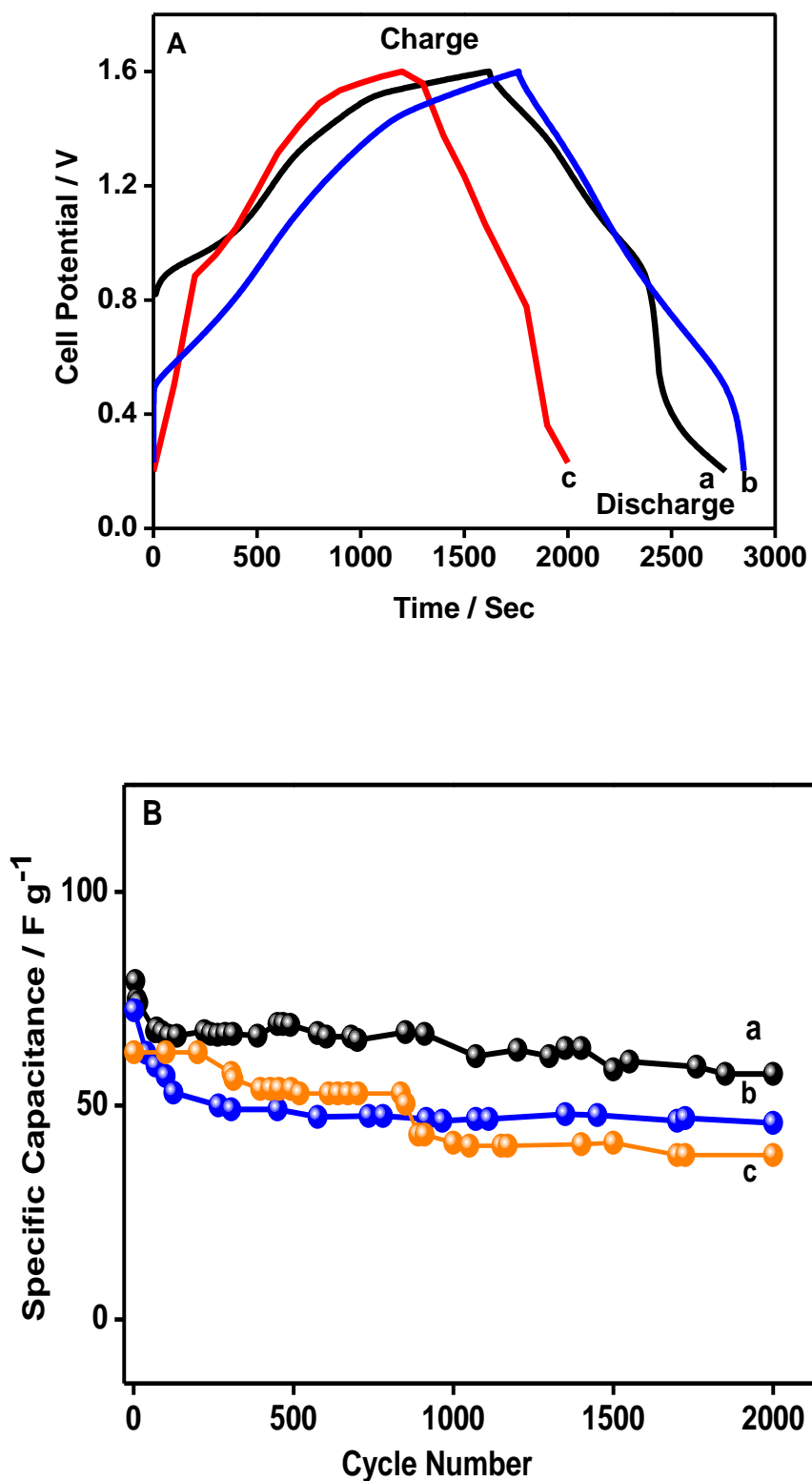
in the presence of optimised surfactant loading 1.0.
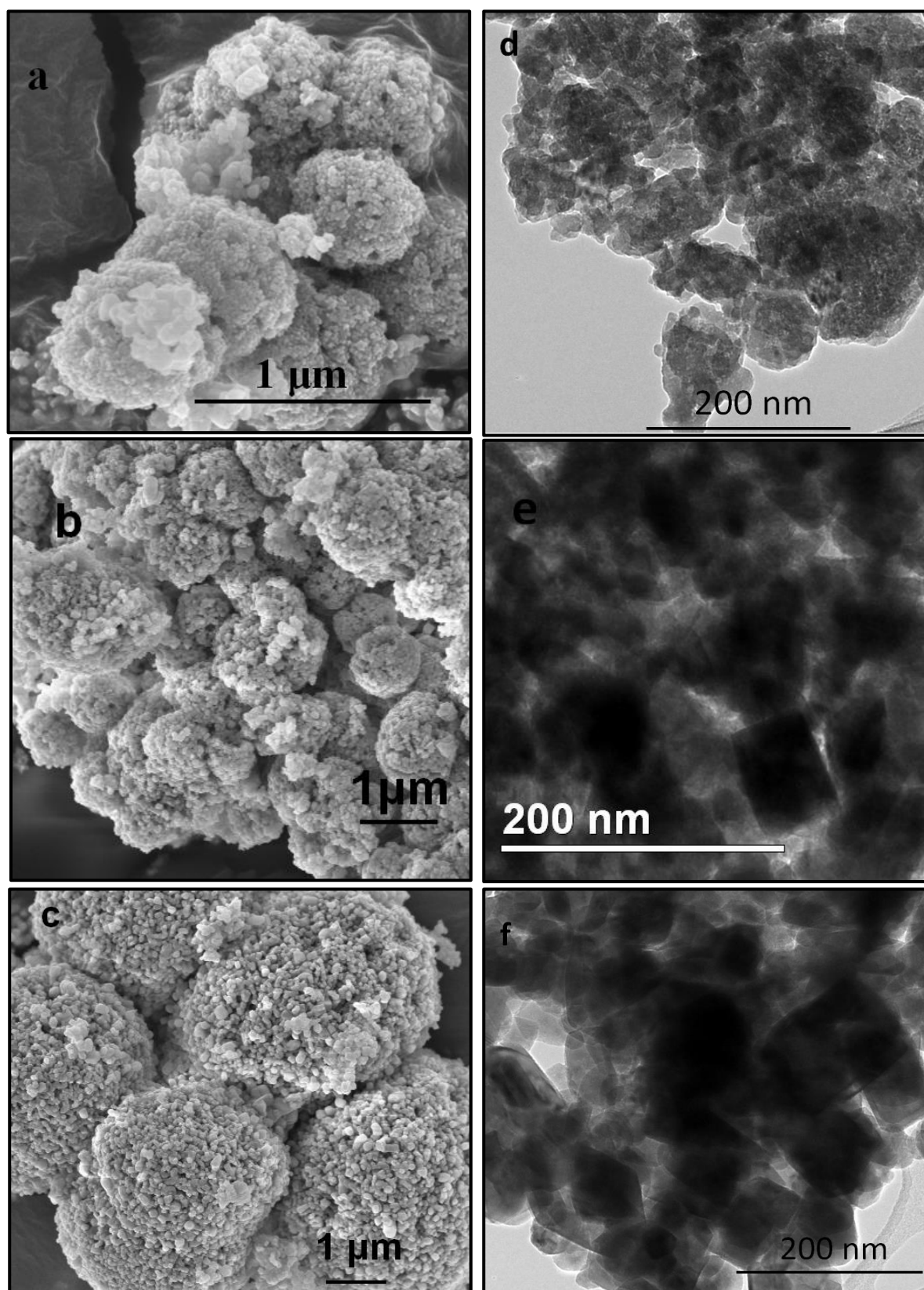
Figure 12 (a-b) FESEM and (d – f) TEM imaging of CoMoO$_4$ materials synthesised at (a, d) 300, (b, e) 400 and (c, f) 500 ^{o}C in the presence of optimised surfactant loading 1.0.

Figure 13 Cyclic voltammetric (CV) curves (three cell configuration) of CoMoO$_4$ materials synthesized at (a) 300, (b) 400 and (c) 500 ^{o}C in the presence of optimised surfactant loading 1.0 showing data for multiple (50) cycling. (d) First CV curves are compared for three samples.

Fig. 14 (a – c) Charge – discharge behavior of CoMoO₄ (three cell configuration) electrodes and (d – f) cyclic voltammetric curves (CV; two cell configuration), oxidation – reduction behavior of hybrid capacitor AC ‖ CoMoO₄. The CoMoO₄ electrodes synthesized at (a, d) 300, (b, e) 400 and (c, f) 500 °C in the presence of optimized surfactant loading 1.0 are shown.

Figure 15 (A) Galvanostatic charge - discharge (two cell configuration) curves and (B) Variation of specific capacitance *vs.* cycle number of CoMoO$_4$ materials synthesized at (a) 300, (b) 400 and (c) 500 ^{o}C in the presence of optimised surfactant loading 1.0.

Table of Content
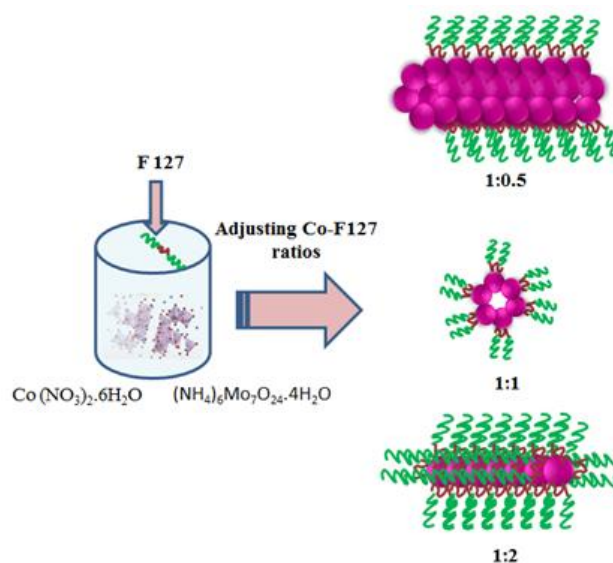
Effect of surfactant content: The formation of nanostructured $CoMoO_4$ materials (purple colour) in the presence of various amounts of F127 surfactant (green strings) loadings (Cobalt metal to surfactant ratios 1:0.5; 1:1; and 1:2). With the variation of surfactant ratio we have tuned the redox properties of $CoMoO_4$ and enhanced the available specific capacitance of this material in aqueous hybrid capacitor.